Applied Geomatics (2026) 18:72
https://doi.org/10.1007/s12518-026-00727-w

RESEARCH

InfraHBIM/HBIM–GIS integration for the reconstruction and remote access of the First Songhua River Bridge heritage complex along the Chinese Eastern Railway (1901–1961)

Jianzhuo Xu[1] · Manuel Garramone[1] · Fangming Li[2] · Haitao Zhang[3] · Marco Scaioni[1]

Received: 13 November 2025 / Accepted: 2 April 2026 / Published online: 20 April 2026

Abstract

The First Songhua River Bridge of the Chinese Eastern Railway (CER) entered service in 1901 and was protected by three military blockhouses constructed between 1915 and 1917. As the first metal bridge in the country exceeding one kilometre in length, the bridge represents a major achievement in the engineering history of the CER. Although the bridge preserves a substantial and diverse collection of historical archives, these materials have not been systematically organised, while archival records for the blockhouses remain scarce. In 1961, the original curved-chord through trusses and deck trusses were replaced and upgraded. To address these issues, this study proposes an Infrastructure HBIM (InfraHBIM) and HBIM–GIS integration methodology for this transport infrastructure heritage to support archival management, documentation, phase-based three-dimensional reconstruction and web-based remote access. The InfraHBIM model of the bridge representing its state between 1901 and 1961 was reconstructed using a forward modelling strategy based on historical archives, while the HBIM models of the blockhouses were developed through reverse modelling driven by point-cloud data acquired by drone photogrammetry. During the integration phase, heterogeneous datasets were organised within a GIS database derived from historical records and field investigations, and the integrated models were published via ArcGIS ® Online to enable interactive visualisation, attribute query and remote access. The proposed approach provides a reusable reference for the digital management of large-scale linear heritage systems such as railways, canals and defensive networks, while supporting professional decision making as well as public interpretation and engagement.

Keywords Infrastructure H eritage Building Information Modelling (InfraHBIM) · HBIM · BIM–GIS integration · First Songhua River bridge · Chinese Eastern Railway (CER) · Historical reconstruction · Remote access

Introduction

The Chinese Eastern Railway (CER), designed by Russian engineers and entered in service in 1901, consists of a main line extending from Manzhouli in the west to Suifenhe in the east via Harbin, along with a southern branch connecting Harbin to Lvshun and Dalian. As an extension of the Trans-Siberian Railway within Chinese territory, the CER served as a crucial transportation link between mainland Russia, the Russian Far East, and the harbour of Lvshun. Today, the railway and its associated cultural heritage (CH) are recognized as significant examples of linear, industrial, and cross-cultural heritage in China (Xu et al. 2023a; Xu and Scaioni 2023b). Russian engineers designed seven large-scale metal truss bridges along the line: the Nen River Bridge, the First Songhua River Bridge, and the Mudan River Bridge on the

✉ Marco Scaioni
marco.scaioni@polimi.it

1 Department of Architecture, Built Environment and Construction Engineering (DABC), Politecnico di Milano, Milan, Italy

2 3D Survey Group, ABC Lab, Department of Architecture, Built Environment and Construction Engineering (DABC), Politecnico di Milano, Milan, Italy

3 Department of Architecture, College of Architecture and Urban Planning, Tongji University, Shanghai, China

Main Line, as well as bridges spanning the Second Songhua River, the Qing River, the Hun River, and the Taizi River on the southern branch (Fig. 1) (Chinese Eastern Railway 190?). Among them, the First Songhua River Bridge stands out as one of the key control projects along the entire line, being the longest, most technically representative, and one of the most challenging to construct.

Despite being designated as a Key Historical and Cultural Sites under National-level Protection in China and extensively studied by researchers and stakeholders, the bridge has still to undergo comprehensive digital preservation. Efforts such as current condition documentation, 3D reconstruction of its historical transformations, and the development of an online historical archive remain unimplemented.

Heritage Building Information Modelling (HBIM) has long been employed to model historical structures. It is demonstrated as a feasible solution for complex CH components. Moreover, surveying and mapping technologies, including terrestrial/aerial laser scanning and Structure-from-Motion (SfM) photogrammetric approaches, are popular and have replaced traditional methods to document sites (Garramone et al. 2023). Furthermore, HBIM can be integrated with Geographic Information System (GIS) to

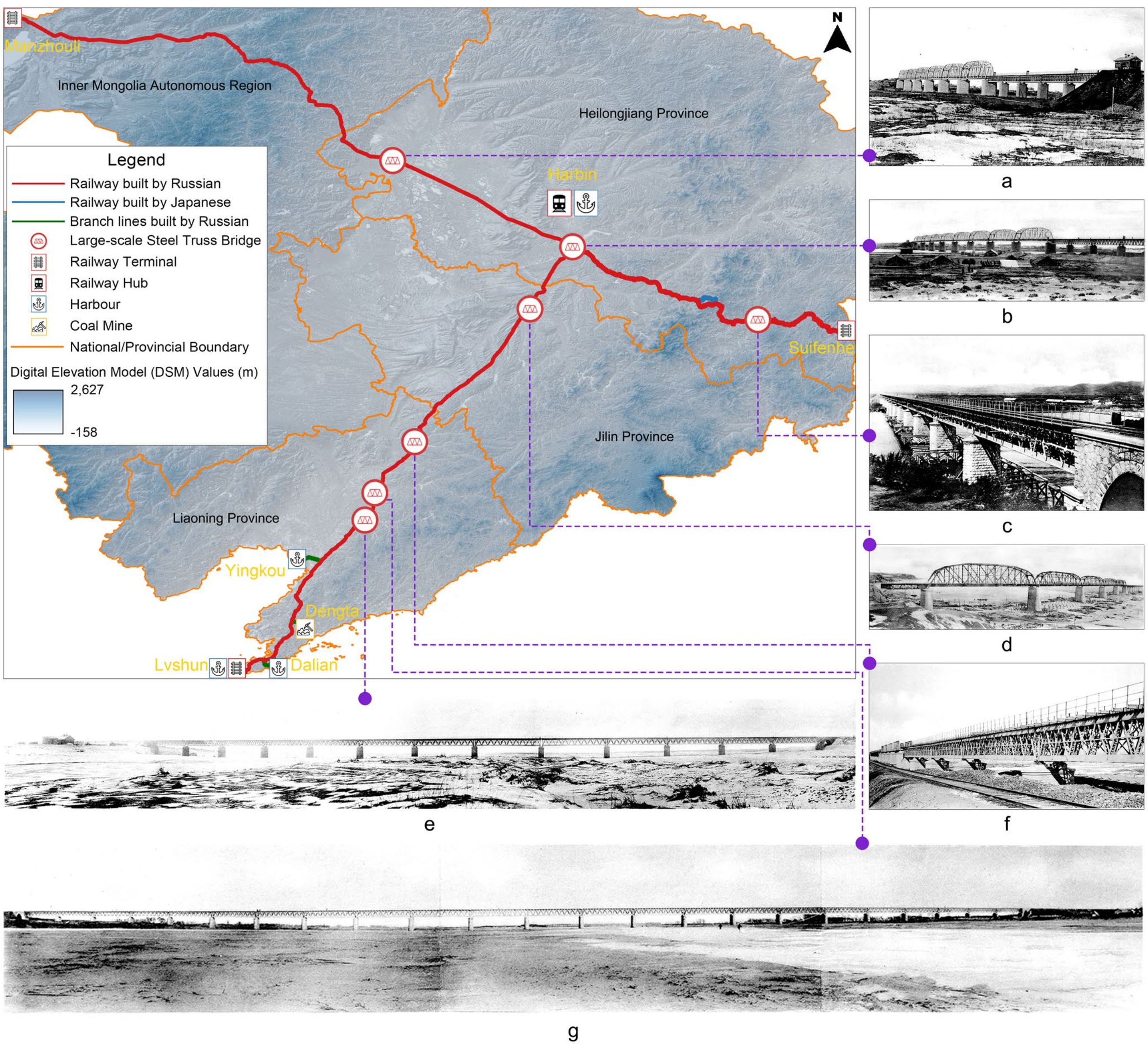

Fig. 1 Layout of the Chinese Eastern Railway (CER) and spatial distribution of its large-scale metal truss bridges: (a) Nen River Bridge; (b) the First Songhua River Bridge; (c) Tieling River Bridge; (d) the Second Songhua River Bridge; (e) Qing River Bridge; (f) Hun River Bridge; and (g) Taizi River Bridge (Chinese Eastern Railway 190?; European Space Agency 2024; National Geomatics Center of China 2025).

record, manage, maintain, and remote access to heritage assets characterized by a wide geographic distribution and constructed/transformed along multiple historical periods.

This study aims to develop a digital database that leverages the potential of HBIM-GIS integration to support archival management, documentation, 3D reconstruction, and remote access for the public to the First Songhua River Bridge and its three military blockhouses along the CER from 1901 to 1961 (Fig. 2).

HBIM for transport infrastructure heritage

Building Information Modelling (BIM) is recognised as an important technology for the digital representation of new constructions. It stores all relevant information through the entire lifecycle, from design and construction to management, demolition, or regeneration. Because of its interdisciplinary and collaborative nature, BIM has attracted wide attention in heritage conservation (Murphy et al. 2009). Moreover, HBIM shows strong potential in the preservation of the built heritage and the digital reconstruction of complex historical structures (Arayici et al. 2017; Antonopoulou and Bryan 2017).

For documenting existing heritage sites, terrestrial and aerial laser scanning and SfM photogrammetry are now widely used. These techniques are faster, more efficient, and more accurate than traditional surveying and mapping methods (Luhmann et al. 2020). Various types of external data, such as point clouds, images, design drawings, geographical data, and Industry Foundation Classes (IFC) files, can be imported into 3D modelling software. This integration allows accurate digital reconstruction and supports the archival storage of CH (Cursi et al. 2022). These methods make it possible to model historical assets precisely and to reconstruct vanished elements from historical records.

Compared with many architectural heritage sites, the conservation and documentation of transport infrastructure heritage (TIH) are often neglected. TIH includes bridges and tunnels that were built to cross difficult terrain. Their conservation and documentation are challenging because of the large-scale distribution, structural diversity, and complex historical evolution of these sites. Researchers must also have interdisciplinary knowledge. These structures are at risk of serious damage or even permanent loss caused by corrosion, human demolition, vandalism, or heavy loading that exceeds their original design capacity. Despite these difficulties, applying HBIM to TIH is essential. It supports the protection and monitoring of heritage sites that still serve their original function. It also helps preserve and reuse decommissioned structures and can reveal and reconstruct important vanished heritage. The transition from HBIM to Infrastructure HBIM (InfraHBIM) is now evident. This new approach also provides a basis for the sustainable development of TIH.

InfraHBIM is used for different purposes. It supports high-precision parametric modelling (Donato et al. 2017), documentation (León-Robles et al. 2019), structural-health evolution and monitoring (Previtali et al. 2019), and management (Bouzas et al. 2022; Barrile et al. 2020). It also enables the use of visual programming languages (VPL) in 3D software to reconstruct vanished sites (Di Donato et ·al. 2022). InfraHBIM is an essential component of HBIM-GIS integration (Xu et al. 2024). Garozzo and Santagati (2021) showed that this approach has created a shared knowledge base that improves cooperation between specialists. HBIM is not only a tool for managing collected information but also a way to preserve the historical memory of structures. It is an operational tool for planning conservation and future maintenance (Conti et al. 2022). It also helps explain historical changes in the built environment (Gómez et al. 2024).

InfraHBIM is widely used in Europe, especially in Italy and Spain. Table 1 presents several study cases and summarises their adopted methodologies. The Level of Development (LOD) (Autodesk, Inc. 2025a) is not defined in many studies. However, the results show that most projects reached a detailed modelling level suitable for reconstructing complex geometries and structural elements. The LOD defines the geometric and informational complexity of BIM models. It is divided into five levels, from LOD 100 to LOD 500 (Table 2) (American Institute of Architects (AIA) 2013). InfraHBIM has been applied to many existing and vanished bridges along roads,

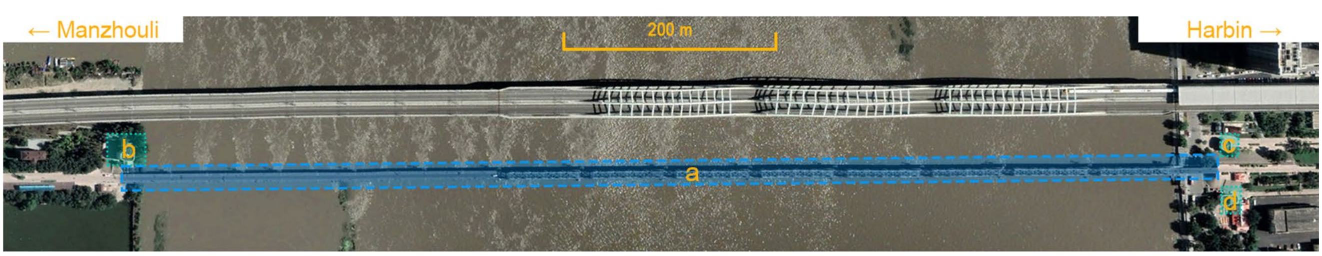

Fig. 2 The spatial relationship between the First Songhua River Bridge and its three blockhouses: (a) the First Songhua River Bridge; (b) Manzhouli-side blockhouse; (c) Harbin-side northern blockhouse; and (d) Harbin-side southern blockhouse (map source: Google Earth Pro).

Table 1 Comparison of Infrastructure Heritage Building Information Modelling (InfraHBIM) implementation cases.

Cases study	Construction Year	Status	Original Function	Structural Type	Data Acquisition Method	HBIM Methodology and Modelling Software	The LOD Employed
The Italian Azzone Visconti Bridge (Previtali et al. 2019)	1336–1338	Remaining	Road bridge	Masonry arch bridge	-Laser scanning -Photogrammetry	-Point cloud and NURBS based -Autodesk® Revit® and Graphisoft Archicad®	Showing a high level
The Spanish Serranos Bridge (Gómez et al. 2024)	1518	Remaining as a pedestrian bridge	Road bridge	Masonry arch bridge	-Archives based -Terrestrial Laser Scanning (TLS) -Photogrammetry	- Point cloud based - Parametric 3D modelling	300–500
The Italian Carlo III bridge (Conti et al. 2022)	18th Century	Remaining	Aqueduct	Masonry arch bridge	-Laser scanning -Terrestrial and UAV photogrammetry -Total station and GNSS	-Point cloud based -Autodesk Revit	Showing a high level
The Italian Giorgini Bridge (Donato et al. 2017)	1827–1828	Remaining	Road bridge	Steel truss bridge	-Terrestrial and UAV photogrammetry -Total station and GNSS	-Point cloud based -Autodesk Revit	Showing a high level
The Spanish Ízbor Bridge	1860–1866	Remaining	Road bridge	Masonry arch bridge	-Archives analysing -TLS	-Point cloud based -Autodesk Revit	300
Italian railway bridges spanning the Po River (Di Donato et al. 2022)	1863–1892	Vanished	Railway bridge	Steel truss bridge	-Archives analysing	-Grasshopper® -Autodesk® Dynamo® for parametric design tools -Visual Programming Language (VPL) within proprietary BIM or 3D CAD software	Showing a high level
The Spanish O Barqueiro Bridge (Bouzas et al. 2022)	1891–1901	Remaining	Road bridge	Riveted steel arch bridge	-Archives analysing -Laser scanning -Visual inspection	-Point cloud based -Autodesk Revit	Showing a high level
The Italian Circumetnea Bridge (Garozzo and Santagati 2021)	1889–1895	Remaining and still-in-use	Railway bridge	Masonry arch bridge	-Laser scanning -Terrestrial, video and UAV photogrammetry	-Automatically segmenting point cloud based -Deep learning -Semi-automatic creation	Not defined
Bridges spanning the Yalu River and the Heshi Lake (Xu et al. 2024)	1897–1901	Vanished	Railway bridge	Steel plate girder bridge and truss bridge	-Archives analysing	-Autodesk Revit	300
The Portuguese Lapela Bridge (Rio et al. 2020)	1915	Remaining and converted into a greenway	Railway bridge	Steel truss bridge	-Archives analysing -TLS -Visual inspection	-Point cloud based -Autodesk Revit	Showing a high level
The Italian Annunziata Viaduct (Barrile et al. 2020)	1970	Remaining and still-in-use	Road bridge	Pre-stressed reinforced concrete	-Archives analysing -Terrestrial and UAV photogrammetry	-Point cloud based -Machine learning -Autodesk Revit	Not defined

railways, and aqueducts. Laser scanning and photogrammetry, carried out using terrestrial or drone platforms (Granshaw 2018a), are the most common data acquisition methods. There is no standard workflow, but most projects follow the general HBIM methodology and use similar commercial software. Artificial intelligence (AI) technologies, including machine learning and deep learning, have also been introduced in the modelling process (Matrone et al. 2023b).

HBIM-GIS integration in cultural heritage conservation

In recent years, the integration of HBIM-GIS has shown several advantages in improving the conservation and management of CH. HBIM supports complete reality-based and parametric modelling. It also provides information on attributes, materials, and relationships among sub-elements. In addition, it offers insights into potential deterioration

Table 2 Main characteristics of "Level of Development" (LOD) levels (American Institute of Architects (AIA) 2013).

LOD Levels	Stage	Model Element Content Requirements	Authorized Uses
LOD 100	Conceptual Stage	Basic information: a symbol or other generic representation	Analysis; cost estimating; schedule
LOD 200	Schematic Stage	Basic information: approximate quantities, dimensions, shape, location, orientation. Additional information: non-graphic information.	Analysis; cost estimating; schedule; coordination
LOD 300	Detailed Design Stage	Basic information: quantity, size, shape, location, and orientation. Additional information: non-graphic information.	
LOD 400	Fabrication Stage	Basic information: size, shape, location, quantity, and orientation with detailing, fabrication, assembly, and installation information. Additional information: non-graphic information.	
LOD 500	As-Built Stage	Basic information: size, shape, location, quantity, and orientation. Additional information: non-graphic information.	

and changes (Yang et al. 2020). GIS has strong potential in managing, querying, and analysing spatial elements. It can also serve as a visualisation tool, construct and manage databases, collect information, and model large-scale sites.

The integration process is linked to a fundamental challenge. BIM and GIS use different information models: IFC for BIM and CityGML (City Geography Markup Language) for GIS. This difference creates several problems, including the lack of unified standards for defining and converting between the Level of Detail (LoD) in GIS and the LOD in BIM. Other issues relate to geometric/semantic data, and reference systems (Zhu and Wu 2022). In GIS, LoD represents the parameters used to evaluate the semantic accuracy of a HBIM model in a GIS environment, ranging from levels LoD0 to LoD4. Higher levels indicate greater accuracy and more complex 3D objects (Carrasco et al. 2022).

Integration methodologies can be divided into three main approaches: BIM-oriented, GIS-oriented, and balanced BIM-GIS solutions (Garramone et al. 2020). Each group contains several implementation strategies (Wang et al. 2019). At present, there is no standard workflow for HBIM–GIS integration. Two main methodologies have been proposed. One focuses on software interoperability, and the other relies on data conversion. Some studies have used interoperable software such as ArcGIS® Pro, Autodesk® Revit®, and Autodesk®InfraWorks® (Pepe et al. 2021; Barazzetti 2021; Pozzoni et al. 2024), or WebGIS platforms (Bruno et al. 2020; Matrone et al. 2023a). Other researchers have explored data conversion techniques. Examples include transforming IFC files into ESRI Shapefiles using FME® Workbench (Xu et al. 2024) or using the BIMData Platform (Garramone and Scaioni 2023). Recent studies have also evaluated the loss of geometric and informational data that can occur in both integration methods (Colucci et al. 2020).

TIH faces sustainability challenges, regardless of whether the sites are still in use or have been repurposed (United Nations 2015). Property owners, such as road or railway companies and local governments, seek to reduce maintenance costs while keeping the infrastructure operational. The heritage authorities, on the other hand, aim to ensure minimal intervention to preserve authenticity and structural safety. In addition, heritage sites should provide public and research access. Considering these needs, HBIM-GIS integration offers an efficient solution for the conservation, documentation, and remote accessibility of the infrastructure heritage.

The First Songhua River Bridge along the CER Main Line

The First Songhua River Bridge is located in Harbin, China. Harbin was the only hub and first-class station along the whole CER line. The bridge is the longest and earliest among the seven major truss bridges on the CER, and it has the largest span. It was also the first 1-km-long bridge in China at the beginning of the 20th century, with a total length of 1,003.62 m. The bridge consists of 11 spans (Spans No. 1–10[1] and Span No. 19) with 32.01 m (15 саж[2]) deck trusses and eight spans (Spans No. 11–18) with 74.69 m (35 саж) through-deck curved-chord trusses (Fig. 3). It was designed by Russian engineers and built by Russian and Chinese workers within fifteen months, from May 1900 to August 1901 (Chinese Eastern Railway 190?). The pneumatic caisson technique was used for the pier foundations that support the through trusses. The foundations of the remaining piers and the abutments at both ends were built using the open-caisson method during the low-water season in spring. Straight ramps are located on both the north and

[1] According to the original design drawings, the numbering of the abutments and piers is arranged starting from the side of the bridge closer to Manzhouli (northern side). The abutments on the Manzhouli and Harbin (southern side) sides are numbered 1 and 20, respectively. The piers with open-end caisson foundations are numbered 2 to 10, while those with box caisson foundations are numbered 11 to 19. The numbering of the trusses follows the same rule, sequentially from north to south as 1 to 19.

[2] ‘сажéнь’ abbreviated as ‘саж’, is a historical Russian unit of length, where 1 саж = 2.134 m.

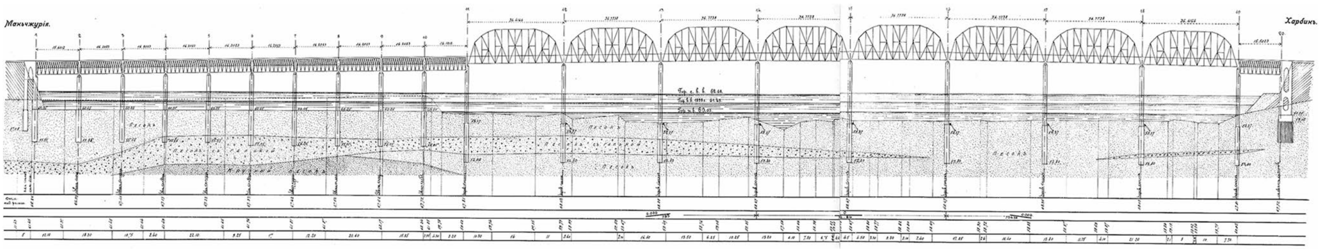

Fig. 3 Initial elevation design of the First Songhua River Bridge, showing the elevation of pier and abutment foundations as well as hydrogeological information (Chinese Eastern Railway 190?).

south sides, connecting the bridge deck. The gradients are as follows: from the starting point of the northern approach to Truss No. 14, the gradient is 0.003 m per 1.68 km; for Trusses No. 15 and No. 14, it is 0 m per 0.16 km; from Truss No. 16 to the endpoint of the southern approach, the gradient is 0.003 m per 1.57 km. The total length from the northern approach to the southern endpoint, including the bridge itself, is 5,614.64 m (Fig. 4). Between 1915 and 1917, the Russian government assigned the military engineer Captain A. A. Rakhmanov to Manchuria to construct a series of defence facilities to protect key infrastructures along the CER, including tunnels, large truss bridges, and loop lines (Avilov 2024) (Fig. 5). Three blockhouses were built to defend the bridge. One concrete blockhouse is on the Manzhouli side and two are on the Harbinside. All three military buildings have parapet sections and shooting holes on four sides, which differ in number and size (Fig. 6).

In the 1960s, the railway administration decided to replace the original trusses and renovate the piers. The decision was due to serious damage caused by floods in 1932, 1956, and 1957 (The Compilation Committee of the Harbin Railway Admission 1999). The through-deck curved-chord trusses were replaced with parallel-chord trusses that included pedestrian walkways on both sides. The pedestrian walkways and their supporting trusses were attached to both sides of the deck trusses. In addition, Pier No. 3 was rebuilt in reinforced concrete without stone cladding, and the cutwaters of Piers No. 8 and No. 11 were strengthened with concrete reinforcements (Fig. 7).

The bridge and its three blockhouses have been listed as major historical and cultural sites protected at the national level in China since 2013 (Code No. 7–1900-5–014) (The State Council of the People's Republic of China 2013). The bridge was closed the following year and was later converted for pedestrian use. Although trains no longer pass over it, the bridge has been preserved through the efforts of many CH stakeholders. Its role in connecting both sides of the city also contributed to its preservation. In addition to its

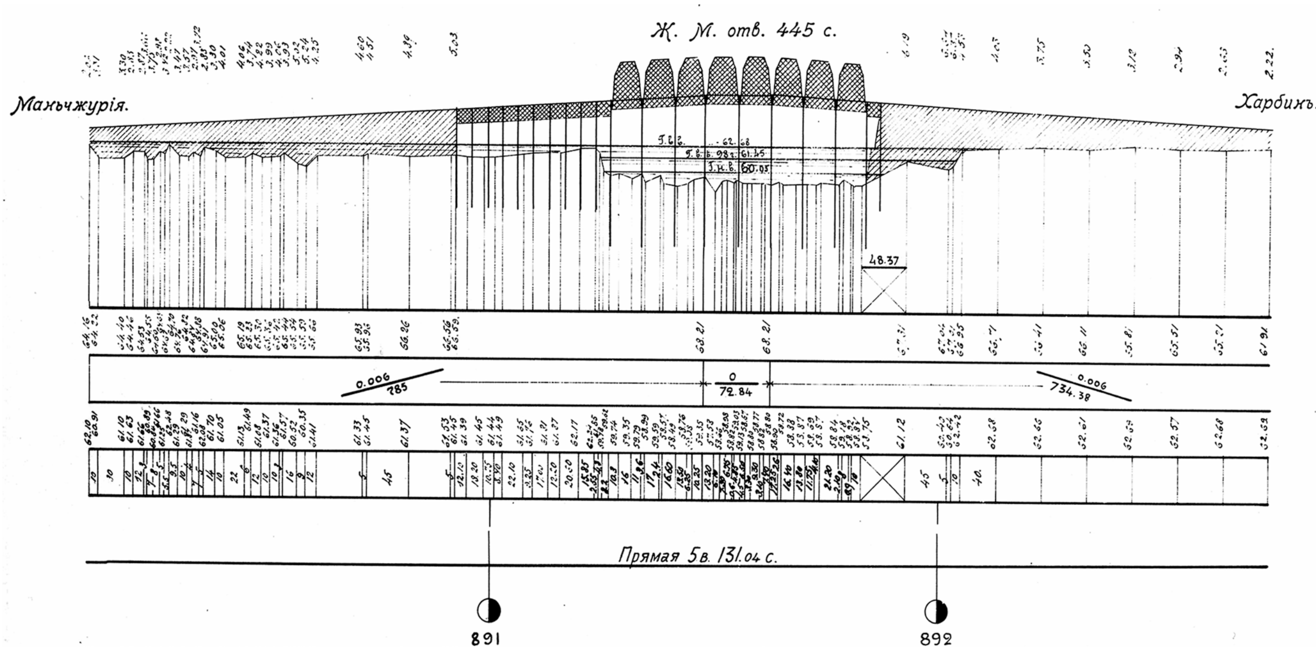

Fig. 4 Longitudinal section and gradient design diagram of the First Songhua River Bridge (Chinese Eastern Railway 190?).

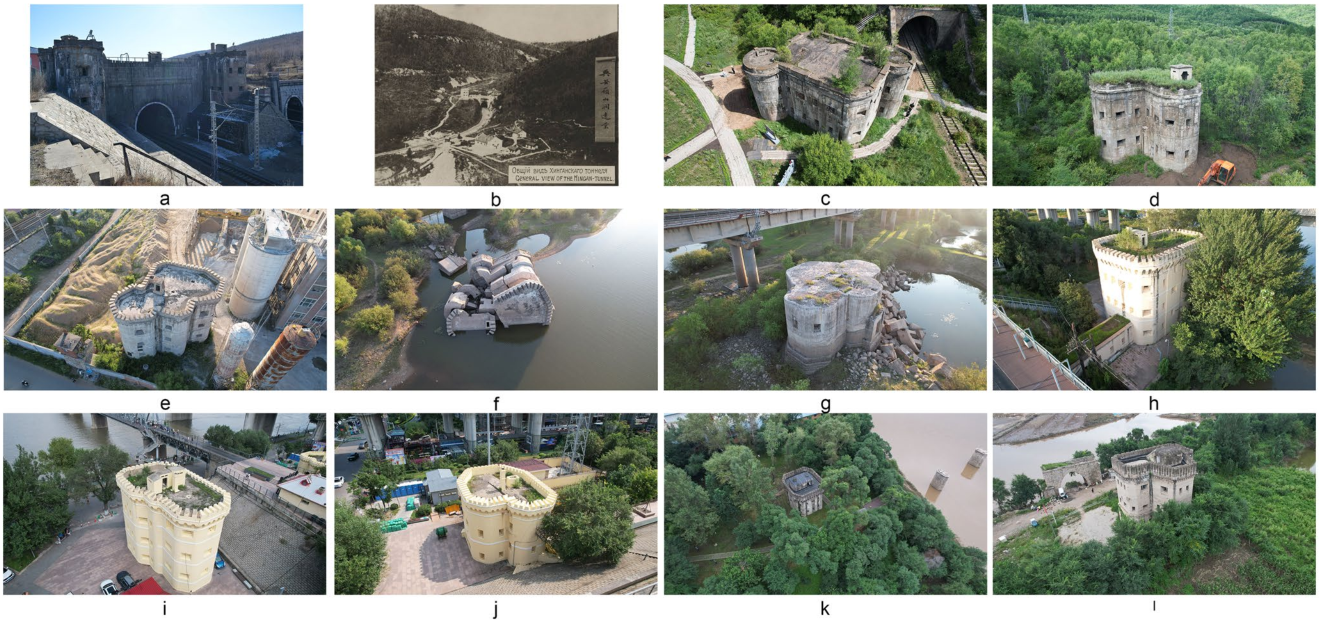

Fig. 5 Blockhouses of the key infrastructural elements along the CER Main Line: (a) Khing'an Range Tunnel Manzhouli-side blockhouse; (b) Khing'an Range Tunnel Harbin-side blockhouse (Anon 1919); (c) Xin'nangou Culvert along the Khing'an Range Loop Line Manzhouli-side blockhouse; (d) Xin'nangou Culvert along the Khing'an Range Loop Line Harbin-side blockhouse; (e) Nen River Bridge Manzhouli-side blockhouse; (f) Remains of the Nen River Bridge Harbin-side northern blockhouse; (g) Remains of the Nen River Bridge Harbin-side southern blockhouse; (h) the First Songhua River Bridge Manzhouli-side blockhouse; (i) the First Songhua River Bridge Harbin-side eastern blockhouse; (j) the First Songhua River Bridge Harbin-side western blockhouse; (k) Tieling River Bridge Suifenhe-side blockhouse; and (l) Tieling River Bridge Harbin-side blockhouse.

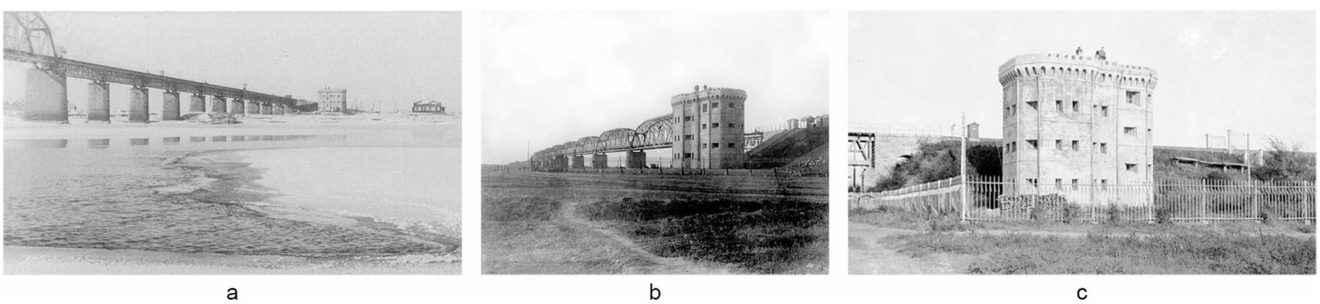

Fig. 6 Photographs taken after the completion of the blockhouses: (**a**) Manzhouli-side blockhouse; (**b**) Harbin-side southern blockhouse Perspective 1; and (**c**) Harbin-side southern blockhouse Perspective 2 (Anon. 2019a, b, c).

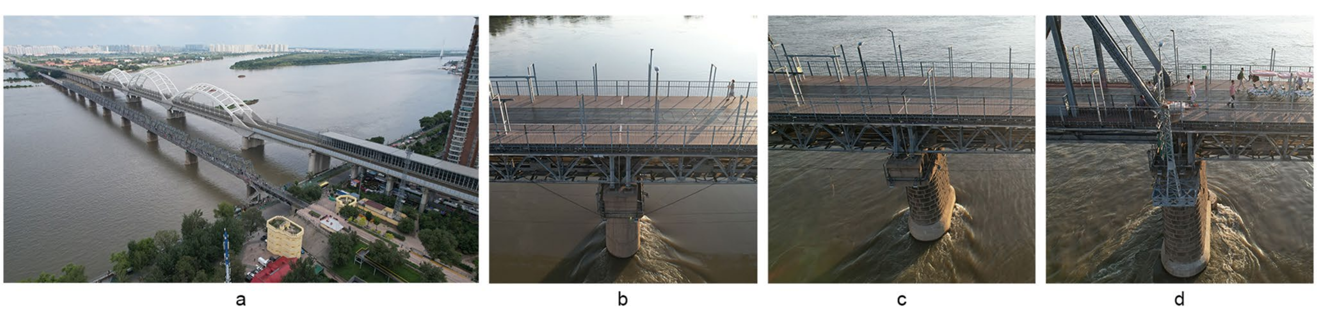

Fig. 7 Condition of the remaining parts of the first Songhua river bridge: (**a**) Overview of the bridge on the Harbin-side; (**b**) Pier No. 3; (**c**) Pier No. 8 and (**d**) Pier No. 11.

functional value, the bridge is considered a key element in the city's development and a symbol of its urban identity.

The significance of this structure not only lies in its historical and cultural value but also in the technical achievements of its construction. It forms an essential part of the CER, a large-scale railway system established in China in the early 20th century. As part of the national strategy for the sustainable development of the infrastructure heritage, comprehensive documentation is urgently required to support more effective management and maintenance. The results may be also shared and applied to other examples of infrastructure heritage along the historic railway.

Methodology and workflow

InfraHBIM/HBIM–GIS integration was selected as the 3D modelling approach to present the historical evolution and remote access of the First Songhua River Bridge and its three blockhouses. Digital images and historical documentation from 1901 to 1961 were collected and organised. Because the historical records of the blockhouses are almost absent, data acquisition was performed using drone-based photogrammetry in summer 2024. The methodology consists of six main steps. These include: (1) archival collection and analysis, (2) GIS database development, (3) data acquisition and processing, (4) InfraHBIM/HBIM construction and geometric accuracy evaluation, (5) InfraHBIM/HBIM–GIS integration, and (6) remote access implementation (Xu et al. 2025b). The workflow is shown in Fig. 8, and each step is described in the following subsections.

Archival collection and analysis/GIS database development

To enhance the GIS database, the creation of InfraHBIM/HBIM for different periods, and the reconstruction of historical changes, seven sets of historical documents from China,

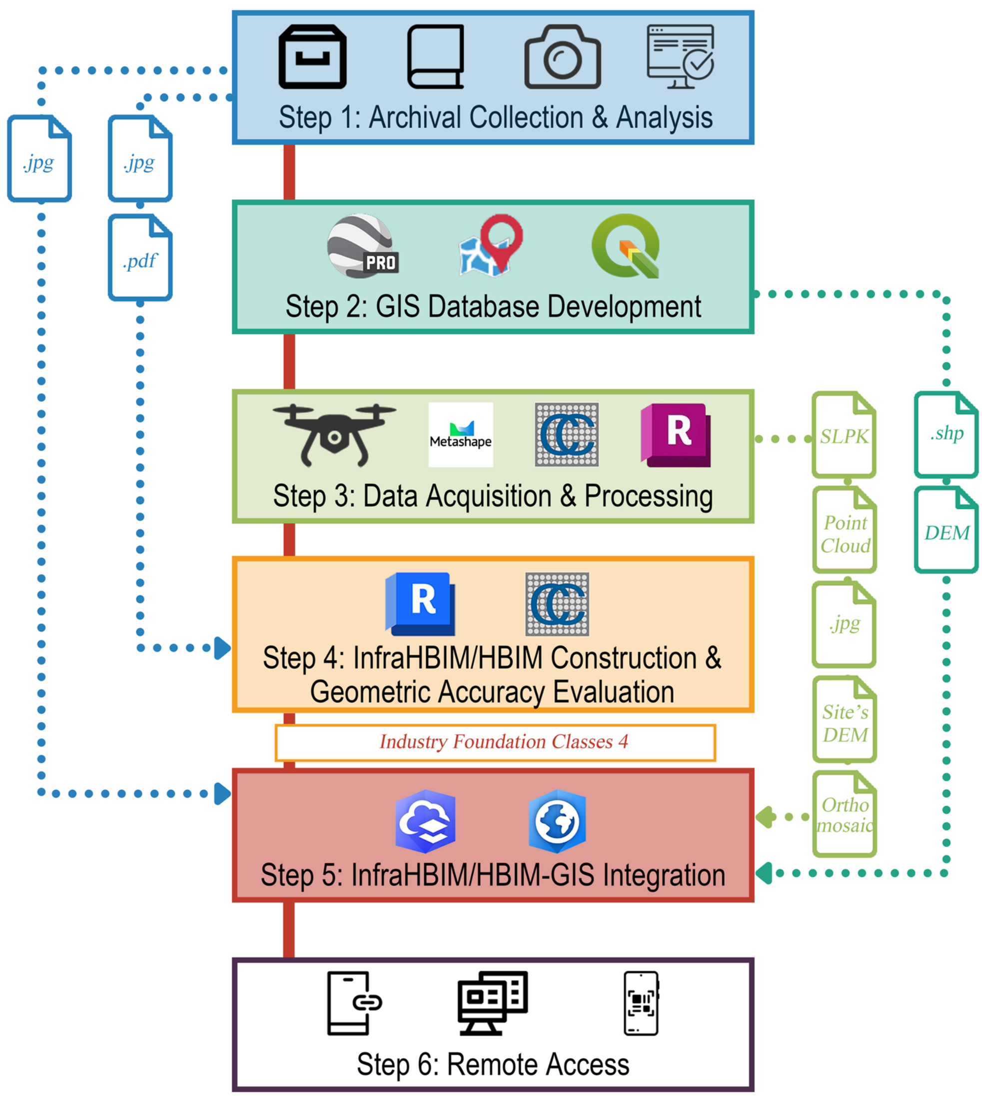

Fig. 8 Workflow of the InfraHBIM/HBIM-GIS integration applied in this study

Russia, Japan, and Singapore were collected and analysed (see the list of these documents in Table 3).

The GIS database construction for the bridge then began. For clear identification and management, each of the four heritage sites was assigned a 12-digit ID code (Xu et al. 2024). The bridge is WLBSTR0892AP. The blockhouse on the Manzhouli side is WLMBHR0892AF. The southern and northern blockhouses on the Harbin side are WLMBHR0892BF and WLMBHR0892CF, respectively. The code includes six components. These consist of the location, the site category, the designer, the mileage, the serial number, and the remaining status, as described in Table 4.

Historical drawings and photographs were organised and classified. Geographic coordinates were exported from Google Earth Pro (Version 7.3.6.10201) (Google 2025) and assigned to the relevant documents using GEOSETTER (Version 3.5.3) (Schmidt 2019). The Digital Elevation Model (DEM) was obtained from Copernicus GLO-30 (European Space Agency 2024). All historical documentation was then imported into QGIS Desktop (Version 3.30.2) (QGIS Association 2023) as vector Shapefile layers (Fig. 9).

Table 3 Archives collected and used for the analysis in this study.

Historical Archives Title	Date	Type	Archive sources
Album of structures and standard drawings of the Chinese Eastern Railway, 1897–1903 (Chinese Eastern Railway 190?)	1897–1903	Album	National Library of Russia
Album of the construction of the Chinese Eastern Railway, 1897–1903 (Anon 1904)	1897–1903	Album	Library of the Russian Geographical Society
Album of views of the Chinese Eastern Railway (Phot. Khosita (фот. Хосита) 1901)	1901	Album	National Library of Russia
China Eastern Railway (Podolsky 1910)	1910	Album	National Library of Russia
Views of the Chinese Eastern Railway (Anon 1919)	1903–1919	Album	Singapore Management University Libraries
Historical Overview of Chinese Eastern Railway, 1896–1923 (Nilus 1923)	1896–1923	Book	The Presidential Library in Russia
An Lien Bridge Near Harbin[a] (Anon 1920)	1920	Photo	Kyoto University Main Library
Harbin: Iron-bridge of R. Sungarri, Harbin (Anon 1930)	1930	Postcard	Kyoto University Main Library
Historical Records of the Harbin Railway Admission, 1896–1995 (The Compilation Committee of the Harbin Railway Admission 1999)	1896–1995	Book	National Library of China

[a] In certain Japanese historical documents, the name "Harbin" appears in the transliterated form "Harubin."

Table 4 Encoding rules and meaning of the characters in the ID code for infrastructural and affiliated architectural heritage.

Character No.	Meaning of the character	Abbreviation and meaning
1–2	The section/line on which the heritage is built.	WL - Western section of the Main Line
3–5	The heritage's classification.	BST - Steel Truss Bridge MBH - Military Blockhouse
6	Identity of the heritage designer.	R - Russian
7–10	Mileage location of the heritage along the CER in Russian units.	WL - 0000~0894
11	Serial number of the heritage within the same classification in the same verst.	A~Z
12	The heritage's remaining status.	F - Fully remaining P - Partly remaining

Point clouds data acquisition and processing for the blockhouses

The acquisition of geometric data for the blockhouses was constrained by the scarcity of archival documentation as well as several site-specific conditions. First, apart from the three historical photographs shown in Fig. 6, no additional detailed archival records of the three blockhouses have been identified. Second, the site is currently closed to the public, preventing physical access and the acquisition of interior geometric data. In addition, dense vegetation further limits direct measurements and ground-based surveying techniques. Under these conditions, a non-contact data acquisition strategy was required to obtain sufficiently-accurate geometric information despite the restricted accessibility.

Accordingly, drone-based photogrammetry was adopted as the primary method for geometric data acquisition, as it enables efficient data collection in restricted environments while providing dense and reliable three-dimensional information for subsequent modelling and analysis. A DJI Air 2 S equipped with an FC3411 8.38 mm lens was used to capture high-resolution imagery (5472 × 3078 pixels, pixel size 2.63 µm). Considering the height of both vegetation and buildings, image acquisition was conducted along circular flight paths at approximate relative altitudes of 36 m for the northern blockhouse and 26 m for the two southern blockhouses. A total of 55 and 198 photos were collected for the respective sites. All data were referenced to the coordinate system WGS 84/UTM zone 52 N (EPSG:32652). Due the lack of ground control points, the absolute georeferencing

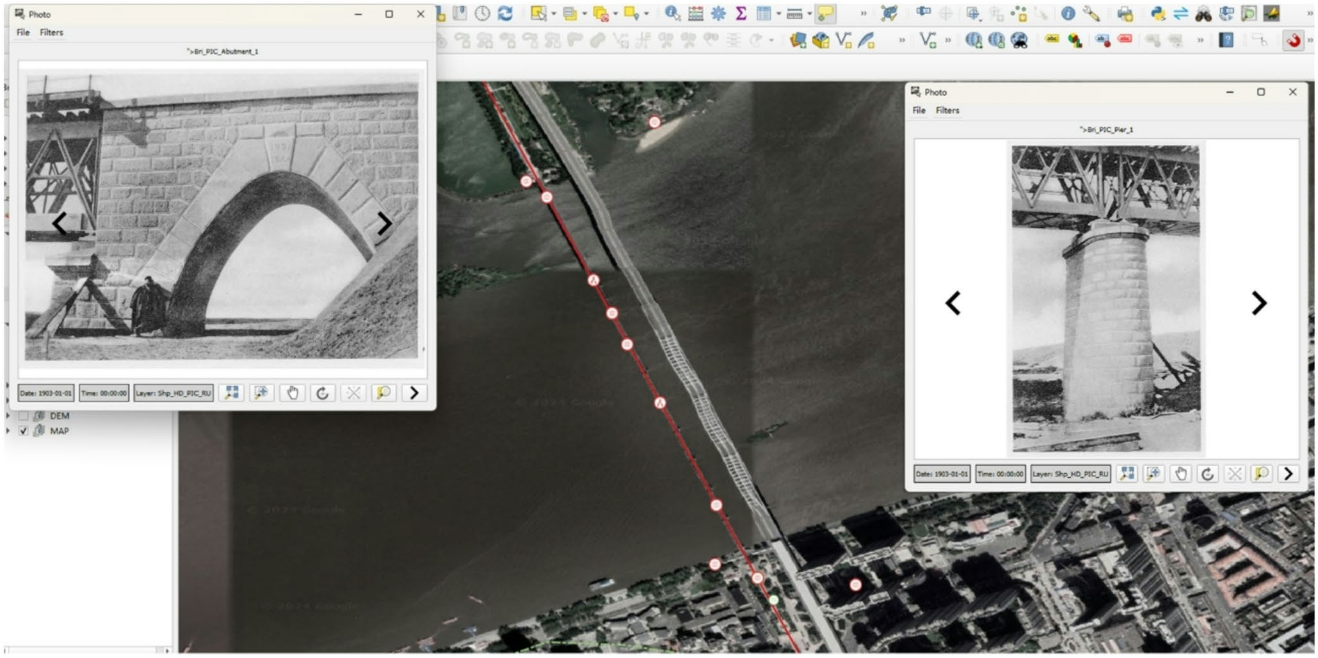

Fig. 9 GIS database of the First Songhua River Bridge.

was carried out using the recorded navigation-grade GNSS data onboard.

Dense point clouds were generated using Structure-from-Motion (SfM) and Multi-View Stereo (MVS) workflow (Granshaw 2018b) implemented in Agisoft Metashape (Version 2.2.0) (Agisoft LLC 2024). After MVS processing, the reconstructed blockhouses yielded approximately 2.84 million and 11.71 million points, respectively. The accuracy and quality of the initial point clouds were evaluated using internal photogrammetric indicators derived from the SfM–MVS processing reports generated by Agisoft Metashape, including image orientation and 3D reconstruction statistics. Table 5 summarises the main accuracy indicators of the initial drone-based photogrammetric point clouds for the three blockhouses, including reprojection errors, camera geolocation errors, ground resolution, dense point cloud size, and point density.

While the indicators reported in Table 5 refer to the initial point clouds generated directly from the SfM–MVS workflow, subsequent point-cloud processing was carried out to improve the usability of the HBIM modelling. The initial point clouds were exported in .las format and further processed in CloudCompare (Version 2.14.alpha) (CloudCompare Development Team 2025) for slicing, denoising, filtering, and elevation-based recolouring. These operations affected point density and cloud size but did not alter the underlying photogrammetric accuracy metrics reported above.

To ensure the compatibility with the HBIM environment, the processed point clouds were converted using Autodesk® Recap® (Ver. 25.1.0.307) (Autodesk, Inc. 2024)

Table 5 Accuracy indicators of the initial drone-based SfM photogrammetric point clouds for the three blockhouses.

Indicator	WLMBHR0892AF (Manzhouli-side blockhouse)	WLMBHR0892BF and WLMBHR0892CF (Harbin-side blockhouses)
Number of images	55	198
Relative flying altitude (m)	36.00	25.70
Ground resolution (cm/pix)	1.1	0.9
Reprojection error (pix)	1.61	1.29
Average camera location error (XY) (m)	0.41	0.54
Average camera location error (Z) (m)	0.26	0.69
Total camera location error (m)	0.49	0.88
Dense point cloud size (points)	2,842,706	11,712,040
DEM resolution (cm/pix)	2.2	1.7
Point density (points/cm²)	0.21	0.37

and subsequently imported into Autodesk Revit (Ver. 2025) (Autodesk, Inc. 2025b) for HBIM creation (Fig. 10). In parallel, tiled models were generated in Scene Layer Package (SLPK) format and imported into ArcGIS® Pro (Esri 2024a) to support large-scale visualisation and subsequent HBIM–GIS integration (Fig. 11). This processing strategy ensured both geometric accuracy and interoperability across

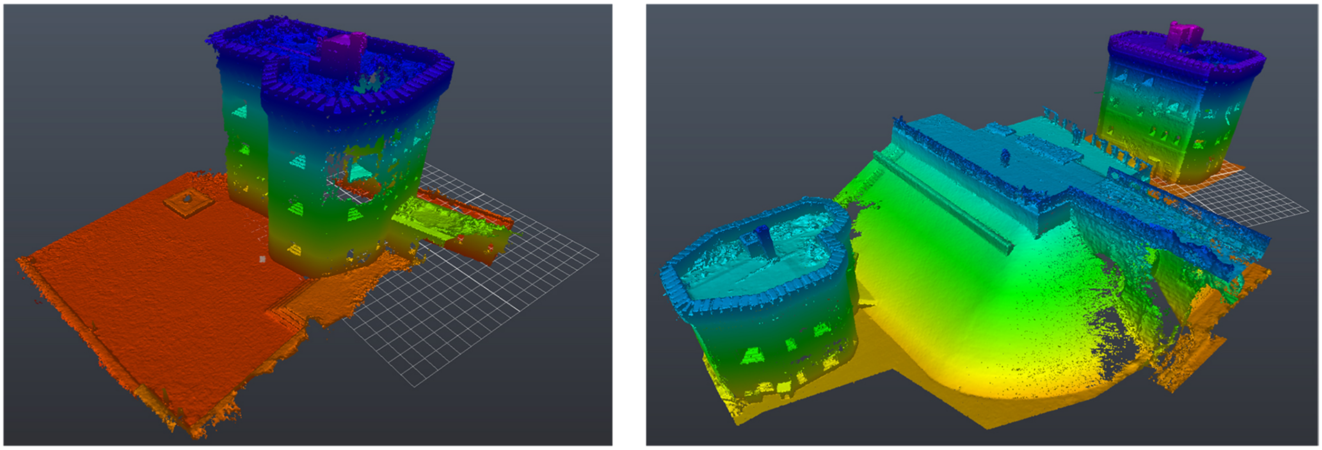

a b

Fig. 10 Processed point clouds used for creating the HBIM models of the blockhouses in Autodesk® Recap®: (**a**) WLMBHR0892AF (Manzhouli-side blockhouse), and (**b**) WLMBHR0892BF and WLMBHR0892CF (Harbin-side blockhouses) with point clouds coloured by elevation.

a b

Fig. 11 Tiled models of the three blockhouses in the Scene Layer Package (SLPK) format: (**a**) WLMBHR0892AF (Manzhouli-side blockhouse), and (**b**) WLMBHR0892BF and WLMBHR0892CF (Harbin-side blockhouses).

modelling and GIS platforms. These processed point clouds provided the primary geometric basis for the subsequent reverse modelling of the blockhouses.

InfraHBIM for the bridge and HBIM for the associated blockhouses

HBIM has become an essential tool for documenting, preserving, and maintaining historical sites by supporting both geometric visualisation and the structured management of heterogeneous information. It serves two main purposes: (i) to support the visualisation of geometry, materials, conditions, and historical changes; (ii) to build a database that integrates multi-source information, including geolocation, historical records, photographs, and structural data.

According to the different heritage types addressed in this study, the bridge was modelled using an InfraHBIM approach due to its infrastructure scale and functional characteristics, whereas the associated blockhouses were modelled using HBIM, given their architectural nature. This distinction enables an appropriate representation of both large-scale infrastructure and building-scale heritage components within a unified digital modelling framework.

Furthermore, significant differences in the availability and richness of the archival documentation between the bridge and the blockhouses led to the adoption of different modelling strategies. The InfraHBIM model was developed using forward modelling (FM), which reconstructs the initial bridge and site based on historical documents (Brumana et al. 2018). In contrast, the HBIM models were created using reverse modelling (RM), which reconstructs the blockhouses directly from point clouds (Xu et al. 2025a, b).

Based on the modelling objectives and available evidence, two historical periods were defined to organise the reconstruction results: 1901–1915, which includes the bridge and the site only, and 1915(1917)-1961, which additionally incorporates the three blockhouses.

InfraHBIM development of the archive-rich bridge through forward modelling

The reconstruction of the bridge required the explicit representation of multiple historical phases while maintaining both modelling accuracy and data manageability within a single digital environment. The main challenges included organising complex structural components across different periods, handling variations in pier elevations that define the bridge's overall arch geometry and controlling the model size and performance during multi-phase reconstruction.

To address these challenges, an InfraHBIM approach was adopted, allowing each structural component to be separately modelled and subsequently integrated into a unified database. The reconstruction process was organised into four methodological steps: (1) reconstruction of the site and riverbed, (2) creation of families for the two truss types, (3) creation of families for the abutments and piers, and (4) assembly of the complete bridge model. Structural families were developed in Autodesk Revit at LOD 300 and exported in IFC 4 (buildingSMART International 2013) format to ensure standardised data exchange .

Specific solutions were implemented to resolve key-modelling issues. Variations in pier height were addressed through vertical adjustments of individual pier families to accurately reproduce the bridge's arch profile. To optimise computational performance and to reduce the size of files, truss models for each span were linked using the Link tool rather than embedded directly. This strategy enabled efficient multi-phase modelling while preserving geometric and semantic consistency. The resulting phased reconstruction of the bridge between 1901 and 1915 is illustrated in Fig. 12.

HBIM development of the archive-scarce blockhouses through reverse modelling

The reconstruction of the blockhouses presented different challenges from those of the bridge, mainly due to their irregular geometry and historically unique defensive elements, which cannot be accurately represented using standard BIM components. Additional difficulties arose from incomplete point-cloud data caused by vegetation cover and the inaccessibility of the interior spaces, which limited the availability of full geometric information.

To address these challenges, a RM-based HBIM strategy was adopted, enabling the reconstruction to be driven primarily by survey data. After importing the point clouds into the selected modelling software, structural components were systematically analysed to identify which elements required the creation of dedicated families and which parts were missing due to data gaps (Fig. 13). The modelling scope included common structures, such as walls and roofs, as well

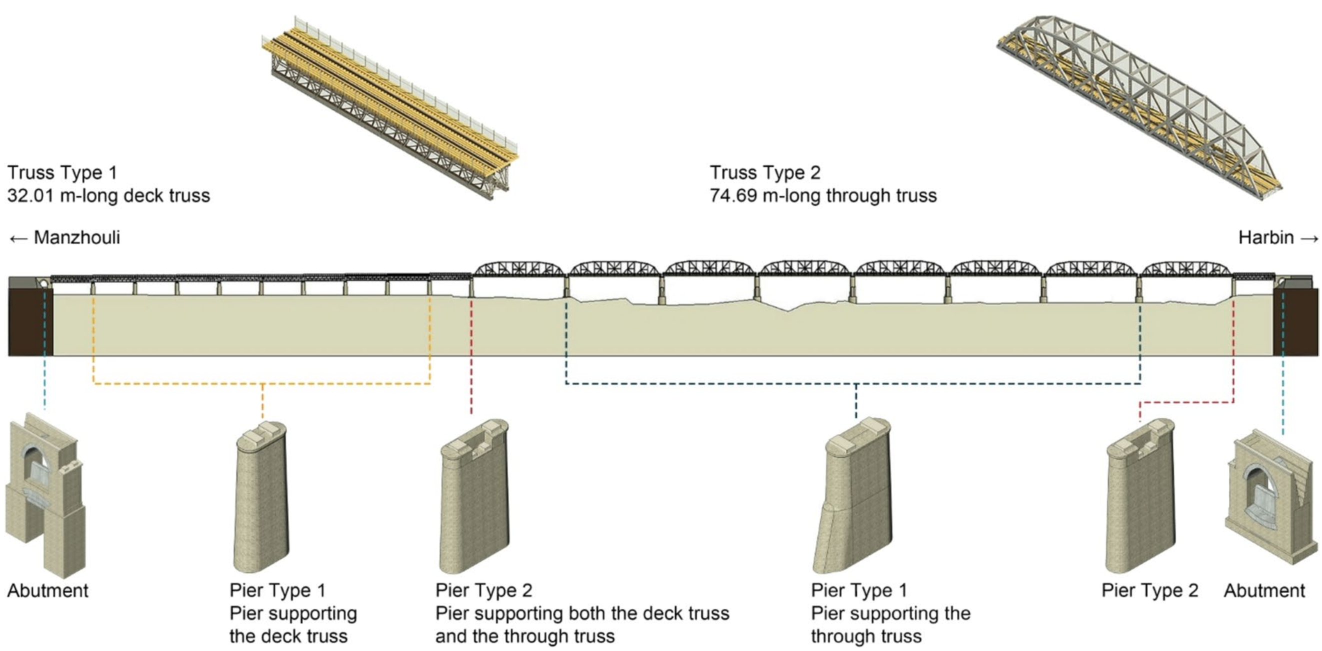

Fig. 12 InfraHBIM and families of the First Songhua River Bridge from 1901 to 1915.

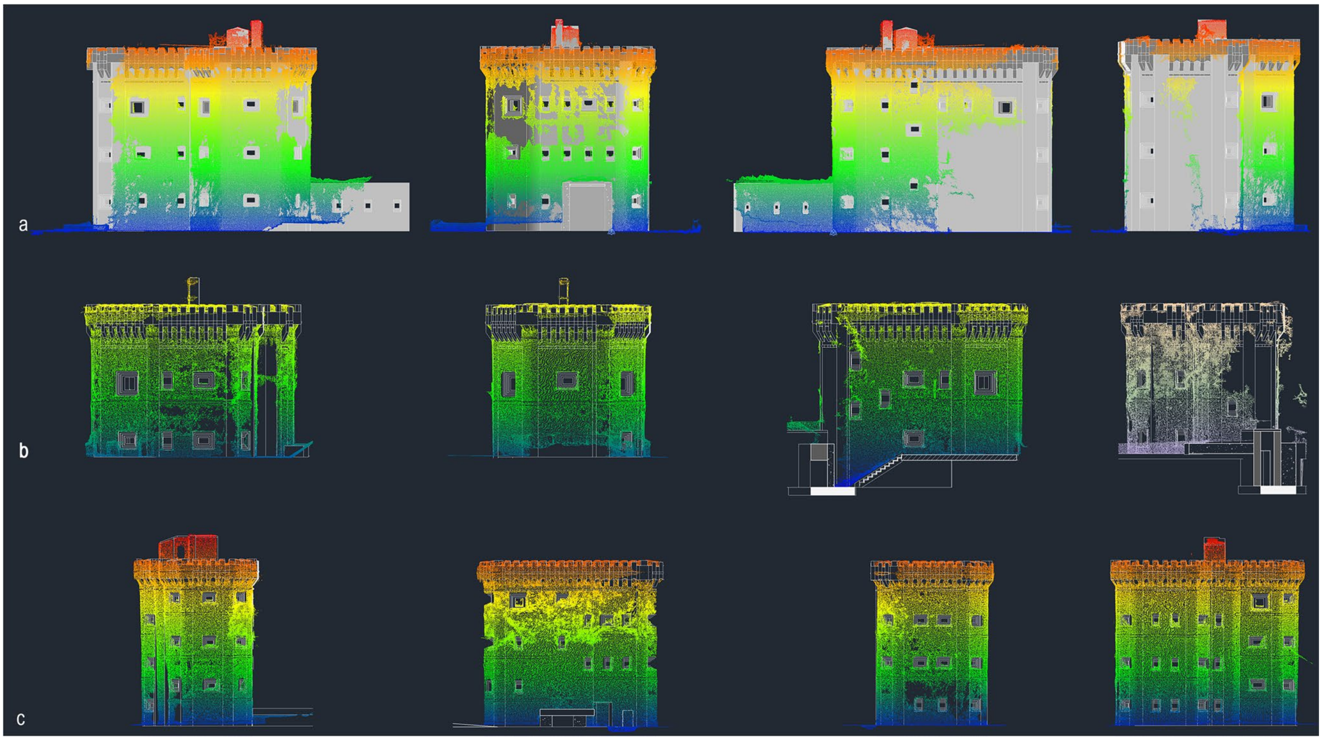

Fig. 13 Gaps in the point clouds caused by vegetation obstruction during the photogrammetric reconstruction of the three blockhouses: (**a**) WLMBHR0892AF (Manzhouli-side blockhouse), (**b**) WLMB-HR0892BF (Harbin-side southern blockhouse) and (**c**) WLMB-HR0892CF (Harbin-side northern blockhouse). From left to right, the north, west, south and east elevations of each structure are shown.

as unique defensive features, including parapets and shooting holes. As interior spaces were inaccessible, they were excluded from the modelling process. Common structures were modelled following standard BIM practices, while unique elements were created as custom families using the Mass tool (Table 6). All elements were classified under IfcBuiltElement in accordance with the IFC 4 standard.

Specific modelling solutions were implemented to ensure an accurate and manageable representation of the blockhouses. Parapets were subdivided into linear segments and corner components. The linear segments were classified into ‘Type A’ and ‘Type B’ based on their spatial position, and each type was further subdivided into ‘Lower’ and ‘Higher’ categories according to façade height. In total, ‘Parapet_A’ included seven lower types and four higher types, while ‘Parapet_B’ included one type. Shooting holes were modelled as four families based on variations in façade width, height, and thickness. Missing elements in the point cloud were reconstructed using photographic references. The resulting HBIM models comprise three blockhouses and support the reconstruction of historical scenes for the period 1901–1961 (Fig. 14).

Geometric accuracy assessment of HBIM models

The quality assessment of the geometric accuracy and completeness of the final HBIM model plays a crucial role to guarantee the reliability of the documentation. On the other hand, since neither ground control points nor distances on the real buildings could be measured, the only possible evaluation consisted in the assessment of the HBIM models against reality-based data, that is, with respect to the photogrammetric point cloud, which is affected by errors. The processing results of the remaining two blockhouses have followed the same methodology and is reported in the Appendix A.

To quantify the uncertainty of the point cloud, the internal precision of the bundle block adjustment (BBA) and the stability of the camera self-calibration have been evaluated. A total of 11,429 tie points has been extracted, resulting in an overall reprojection error after the BBA of 1.61 pixels. The estimation errors of the intrinsic camera parameters, including focal length and principal point coordinates, have ranged between 0.30 and 0.52 pixels, while the distortion parameters showed minor instability. Considering an average ground sampling distance (GSD) of 1.1 cm, we could retain that the relative precision of the point cloud was in the order of 1.3 cm. The average theoretical accuracy of camera absolute geo-location has resulted as 0.41 m in the XY plane and 0.26 m in the vertical direction, yielding a total positional uncertainty of 0.49 m. These metrics reflect the heterogeneous imaging conditions around the blockhouse and indicate that the resulting point cloud is affected by local variations in accuracy.

Table 6 Families created for the blockhouses, including parapet and shooting-hole components.

Details of the families of parapets and shooting holes							
	Wall			Window			
Families	Parapet _A _Lower	Parapet _A _Higher	Parap et _B	Shootinghol e W0866H127 6	Shootinghol eW1276H10 40	Shootinghol eW1642H10 67	Shootinghol eW1707H17 07
	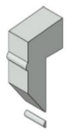		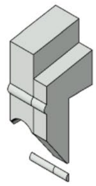	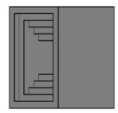	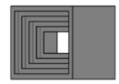	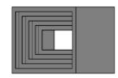	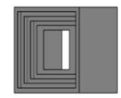
Location	Adapted to a 1000 mm thick wall.	Adapted to a 1000 mm thick wall.	Adapt ed to a 1125 mm thick wall.	Adapted to a 1000/1125 mm thick wall.	Adapted to a 1000/1125 mm thick wall.	Adapted to a 1000 mm thick wall.	Adapted to a 1000 mm thick wall.
Types	Classified based on facade width (mm): L213, L285, L320, L380, L420, L435, L480	Classifie d based on facade width (mm): L320, L380, L435, L480	-	Classified based on wall thickness: T1000, T1125	Classified based on wall thickness: T1000, T1125	-	-

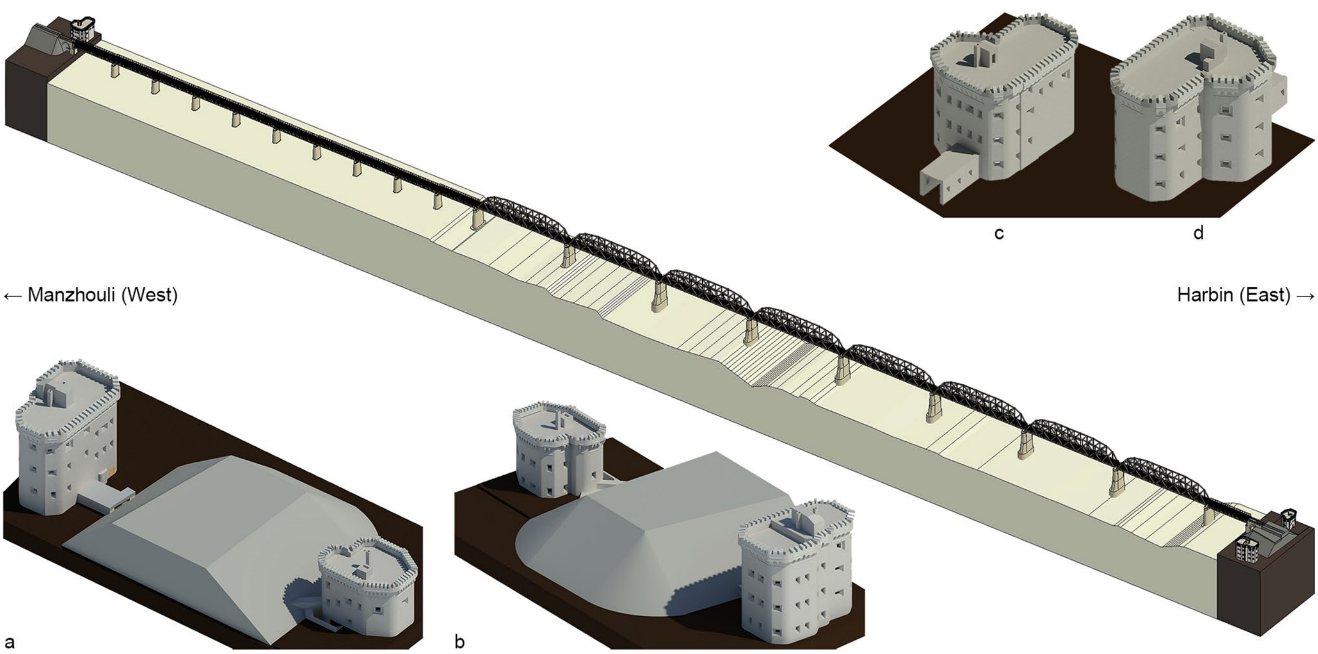

Fig. 14 InfraHBIM models of the bridge and HBIM models of its three blockhouses (1915–1961): (**a**) and (**b**) show the northeastern and southwestern views of the Harbin-side blockhouses (WLMBHR0892BF and WLMBHR0892CF), and (**c**) and (**d**) present the southeastern and northwestern views of the Manzhouli-side blockhouse (WLMBHR0892AF).

Table 7 Bidirectional cloud-to-cloud (C2C) distance analysis between the photogrammetric point cloud (PC1) and the HBIM-derived point cloud (PC2).

C2C direction	Mean (m)	Std. dev. (m)	D_{max} (m)
PC2 → PC1	0.58	0.65	0.80
PC1 → PC2	0.05	0.05	0.25

Moreover, the photogrammetric point cloud (PC1) adopted in this study as data source for the generation of the HBIM model exhibits substantial incompleteness, particularly in the roof sectors, shaded wall regions, and occluded areas. When performing a direct comparison between the HBIM model and the point cloud, these missing regions would be interpreted as large distances, which introduce a pronounced long tail distribution and significantly inflate the overall error (Maset et al. 2025).

To address this issue, a two-stage filtering strategy was adopted to distinguish missing data effects from true geometric deviations. First, a bidirectional Cloud-to-Cloud Distance (C2C) distance analysis was performed after coarse alignment, allowing the identification of the maximum thresholds (D_{max}) used to mask areas dominated by photogrammetric incompleteness. The HBIM mesh has been exported from Autodesk Revit in .obj format and converted into a uniformly sampled point cloud set (PC2) in CloudCompare, while the cleaned PC1 containing 847,397 points served as reference. PC2 has been aligned to PC1 by computing a 3D rigid-body transformation based on the manual measurement of 10 corresponding points. A bidirectional C2C distance analysis was conducted between double point-clouds to separate discrepancies caused by data incompleteness from genuine geometric deviations. The asymmetric behaviour of the PC2-to-PC1 and PC1-to-PC2 distance fields enabled the identification of unreliable areas and the delineation of a valid comparison region for subsequent analyses (Table 7).

After the coarse alignment, an overlap analysis was performed to isolate the reliable common area between PC1 and PC2, and the 50% overlap configuration has been selected for fine registration (Fig. 15).

Second, an overlap-based Iterative Closest Point (ICP – see Pomerleau et al. 2013 for a review on this subject) evaluation was conducted, and the configuration with a validated 50% overlap was selected to isolate the effective comparison region. ICP algorithm has been applied within this valid region, yielding a Root Mean Squared Error (RMSE) of approximately 0.07 m. Based on the thresholds derived from the bidirectional C2C analysis, regions affected by occlusion and reconstruction failures in PC1 were subsequently removed to ensure that the geometric comparison was restricted to spatially reliable areas.

The filtered datasets were then analysed with the Multiscale Model to Model Cloud Comparison (M3C2 - see Lague et al. 2013; Winiwarter et al. 2021) algorithm to ensure that the resulting distances reflect only the actual geometric discrepancies of the HBIM model. The use of a more refined algorithm, which seeks for and computes the distance along local normals, was preferred at this stage to obtain a more precise results, provided that non-overlapping regions have been already discarded.

A core point set of PC1 (PC1_Core) was first generated by spatial subsampling with a minimum spacing of 0.10 m, ensuring a representative and noise-resistant distribution of comparison points. Surface normals were then estimated using a multi scale neighbourhood with a normal scale of 0.20 m to accommodate the geometric variability of the building surfaces. The M3C2 algorithm subsequently computed the signed distances between PC1_Core and PC2 along the normal direction within a search cylinder of 8 cm radius and 1.5 m maximum depth, while incorporating a registration error of 7 cm to account for alignment uncertainty, together with local distance uncertainty estimates (Fig. 16).

Within the validated comparison region, the M3C2 statistics indicate a mean absolute deviation of approximately 0.01 m, a standard deviation of about 0.21 m, and an overall RMSE of roughly 0.21 m. The main distribution of distances lies between −0.40 m and +0.40 m, while the few values outside this range correspond to residual data gaps

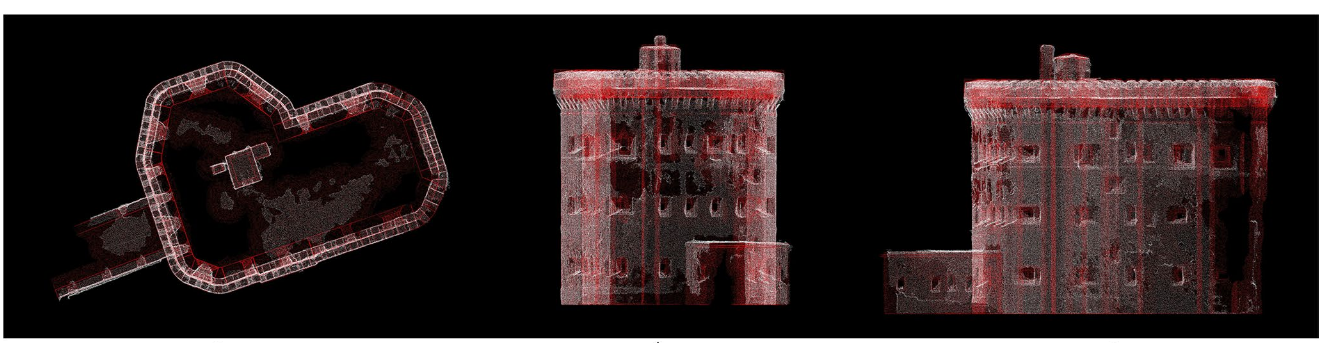

Fig. 15 Extraction of the 50% valid overlap area between the photogrammetric point cloud (PC1) and the HBIM-derived point cloud (PC2), defining the reliable region for geometric comparison: (**a**) Top-view, (**b**) Bridge-facing façade and (**c**) River-facing façade.

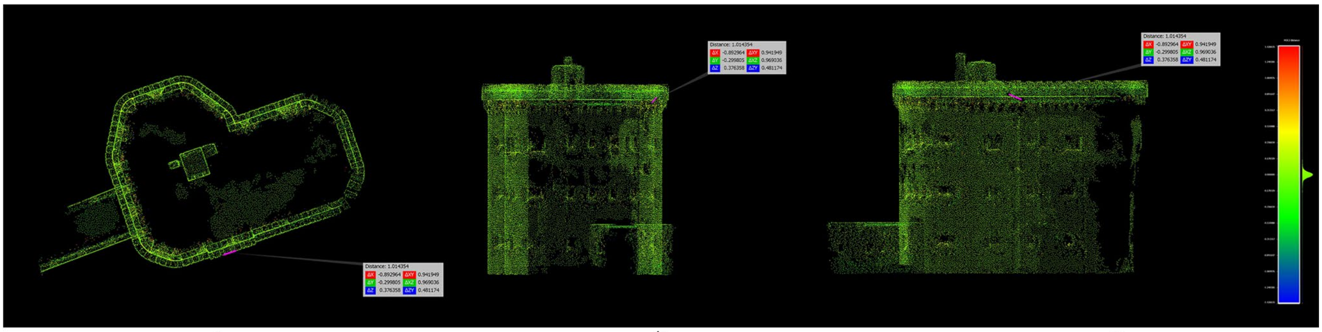

Fig. 16 Multiscale Model-to-Model Cloud Comparison (M3C2)-derived point-to-surface distances between the core point set of PC1 (PC1_Core) and the uniformly sampled point cloud set of PC2: (a) Top view, (b) Bridge-facing façade, and (c) River-facing façade.

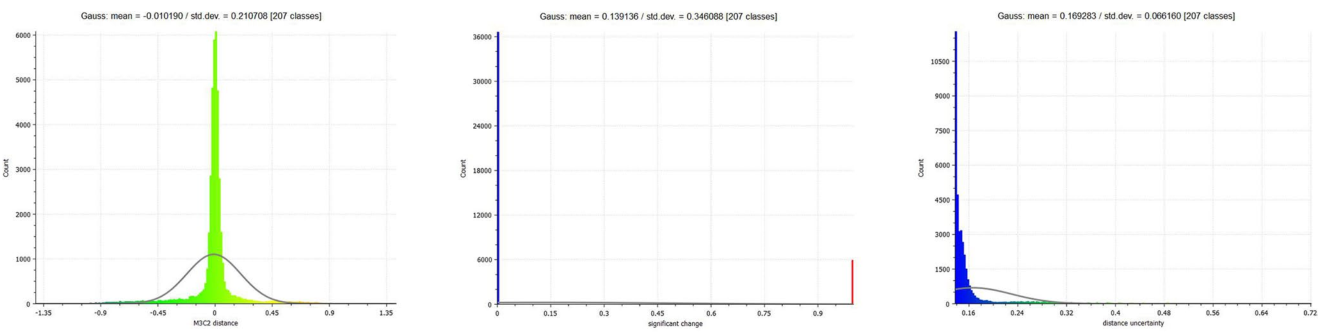

Fig. 17 Multiscale Model-to-Model Cloud Comparison (M3C2)-based geometric analysis results: (a) Distance histogram, (b) Significant change histogram, and (c) Distance uncertainty histogram.

or localized modelling inaccuracies (Fig. 17). These results demonstrate that the HBIM model exhibits a high level of geometric consistency with the photogrammetric point cloud in areas where data coverage is reliable. The proposed two-stage filtering strategy effectively eliminates systematic distortions caused by missing point-cloud data and provides a more robust and reliable assessment of the HBIM geometric accuracy.

InfraHBIM/HBIM-GIS integration and remote access

The InfraHBIM/HBIM–GIS integration developed in this study is based on the unified organisation of multi-source datasets generated in different software environments and subsequently consolidated within a GIS platform. For both historical periods considered (1901–1961 and 1915 (1917)–1961), the InfraHBIM model of the bridge and the HBIM models of the blockhouses were created in Autodesk Revit and exported directly as IFC files using the IFC 4 setup, preserving both component-level geometry and semantic attributes. Geographic coordinates were embedded in the models, and the resulting IFC files were verified in Autodesk® Viewer® (Autodesk, Inc. 2025c) to ensure geometric integrity and attribute consistency prior to GIS integration.

Vector data within the GIS environment were derived from the GIS database constructed in Sect. "Archival collection and analysis/GIS database development", including linear features representing the railway alignment and point features representing bridge components (e.g., steel girders and piers) as well as the spatial locations of the bridge and the blockhouses. These point features were linked to historical archival images through unique URL fields, enabling direct retrieval of the documentary materials.

Point cloud data were exported from CloudCompare in georeferenced .las format and served as a key source of three-dimensional geometric information. Orthophotos and DEMs of the blockhouses were generated in Agisoft Metashape to represent site-scale imagery and terrain conditions. In addition, SLPK models were produced in Agisoft Metashape from the processed point clouds to support efficient 3D visualisation within the GIS environment.

With the exception of image archives, all datasets were ultimately imported into ArcGIS Pro for unified organisation and management. During this process, the IFC files were parsed as 3D feature layers, and their component-level geometry and non-graphic attributes were transferred from IFC Property Sets to the relational attribute tables of the GIS database. This mapping strategy ensured the inheritance and consistent expression of InfraHBIM/HBIM semantic

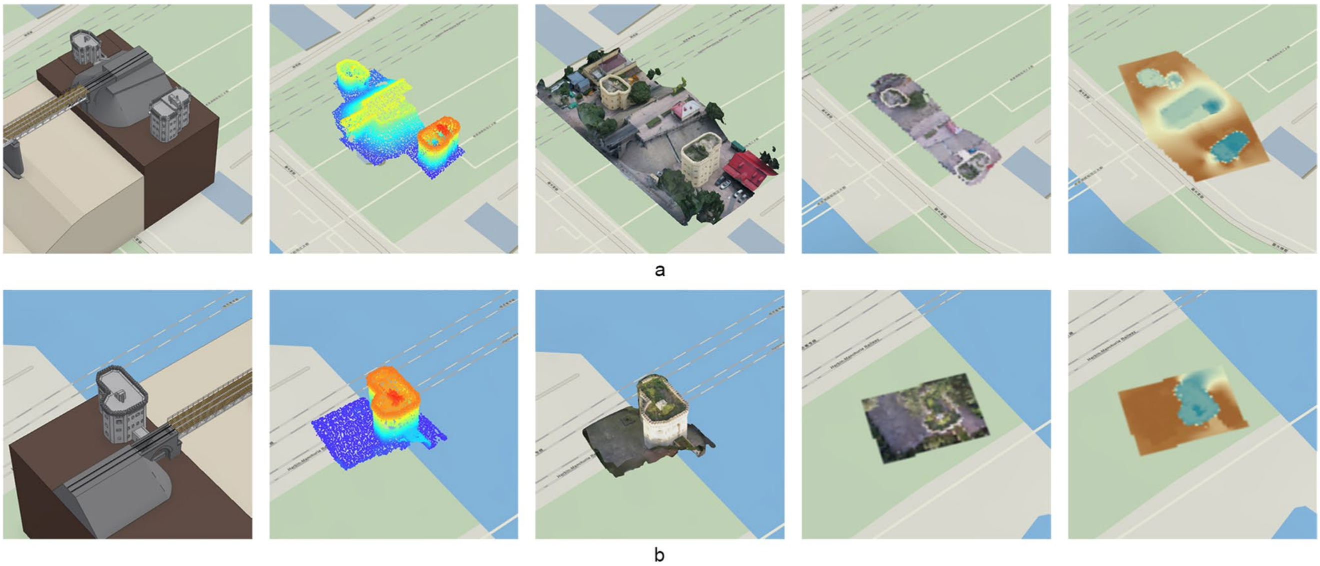

Fig. 18 InfraHBIM/HBIM-GIS integration results in ArcGIS Pro: (a) and (b) show, from left to right, the InfraHBIM/HBIM models, point clouds, Scene Layer Package (SLPK) models, orthographic pictures, and Digital Elevation Models (DEMs).

information within the GIS environment. The integrated models were represented at GIS LoD3, enabling building-scale geometric detail and associated semantic attributes to be visualised, queried, and analysed in a consistent manner, thereby providing a reliable foundation for historical information retrieval and remote-access applications.

The integrated project was subsequently published to ArcGIS® Online (Esri 2024b) using the Web Scene publishing functionality in ArcGIS Pro (Fig. 18). Through the platform, users can browse the integrated results and access archival materials, including historical photographs and on-site documentation images (Fig. 19). At this stage, the InfraHBIM/HBIM–GIS integration workflow is completed. Finally, access links are generated through the platform's sharing functionality, enabling stakeholders to remotely explore and interact with the heritage assets via a web-based interface (https://arcg.is/0aeLyK0).

Conclusion and future work

This study confirmed the value of integrating InfraHBIM and HBIM with GIS for reconstructing and enabling remote access to the historical development of the First Songhua River Bridge and its associated blockhouses along the Chinese Eastern Railway (CER). As a representative engineering achievement within the railway system, the bridge and its defensive structures have experienced substantial structural adjustments, functional shifts, and environmental impacts over more than a century, and they remain key witnesses to the urban development and regional history of Harbin. Before this study, however, their phase-based historical development had not been systematically documented in a digital form. Multi-phase visualisation was limited, and an integrated platform for remote access was not available.

To address this gap, this research combined indirect investigation, including archival research and historical analysis, with direct data acquisition through drone photogrammetry and on-site examination. Multi-phase InfraHBIM models of the bridge and HBIM models of the blockhouses were developed and integrated within a GIS environment. The resulting system organises geographic context, geometric representation, and semantic attributes within a unified digital framework, thereby improving the consistency and manageability of multi-source data. It provides a structured basis for representing, comparing, analysing, and preserving diachronic development across phases. The proposed integration workflow further demonstrates how point clouds, historical archives, and GIS datasets can be coherently organised and delivered through a single platform, offering a reusable technical pathway for the digital documentation and remote accessibility of infrastructure heritage.

The outcomes of this research are intended for multiple user groups, reflecting the spatial characteristics, cultural significance, and representativeness of the First Songhua River Bridge within a broader linear heritage system. At the local scale, the bridge and its blockhouses function as historical landmarks embedded in Harbin's urban fabric and closely connected to community life. The InfraHBIM and HBIM integrated remote-access platform provides local authorities, community residents, and educational institutions with a sustainable digital resource for understanding and managing the heritage. It supports conservation decision making, information management, and public

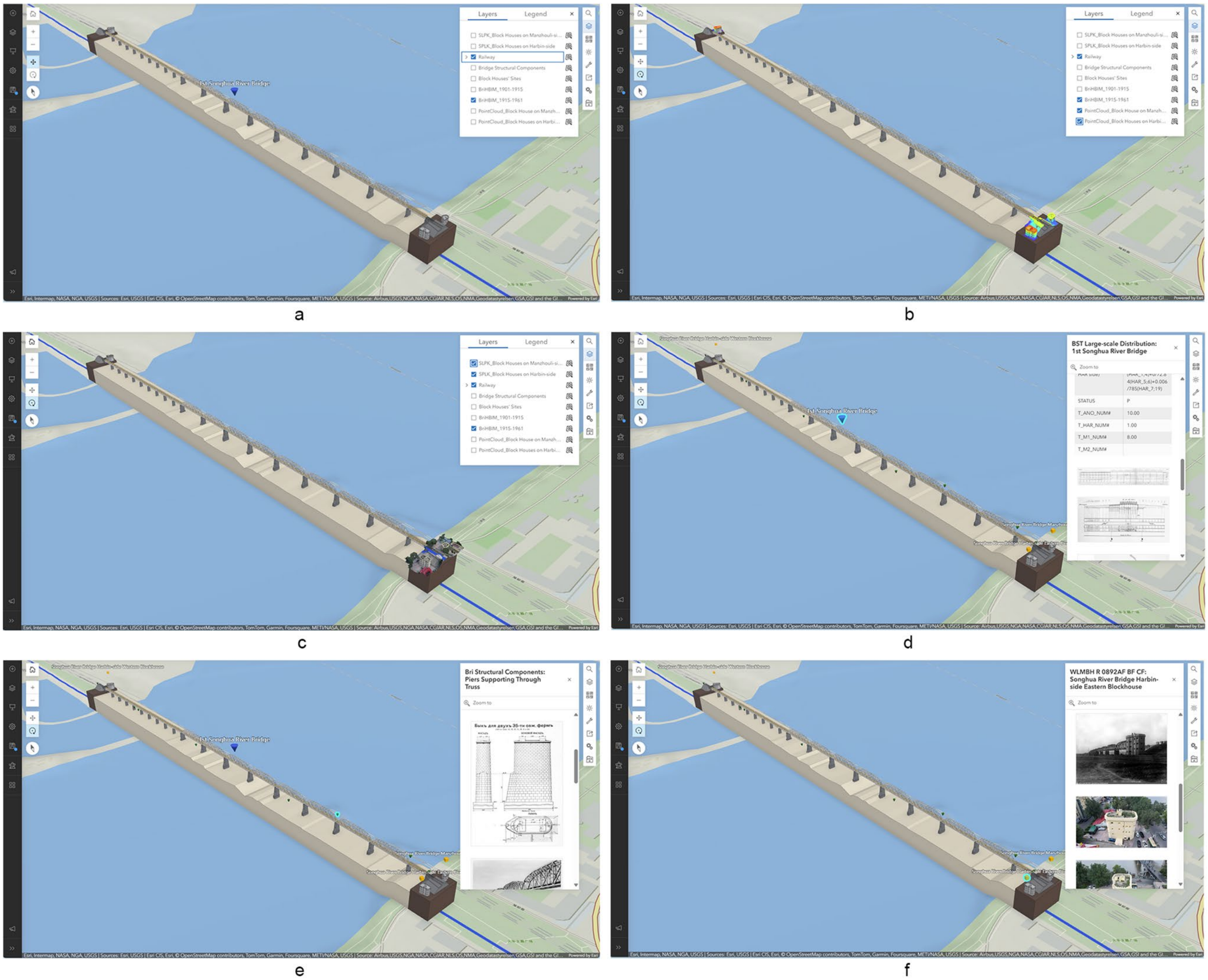

Fig. 19 Integrated results accessed remotely via ArcGIS Online: (**a**) InfraHBIM of the bridge and HBIM of blockhouses; (**b**) point cloud data of the bridge and blockhouses; (**c**) scenes of the bridge and blockhouses in Scene Layer Package (SLPK) format; (**d**) detailed information and historical archives of the bridge; (**e**) historical archives of the bridge piers supporting through trusses; and (**f**) historical archives and current photographs of the blockhouses.

interpretation, while strengthening community awareness and engagement through visualisation and online access. At the broader scale of linear heritage research and management, the CER constitutes a cross-cultural linear heritage system characterised by diverse asset types and wide spatial distribution. By using a technically and historically representative node asset as a validation case, this study proposes an InfraHBIM and HBIM to GIS integration framework that is transferable beyond a single site. It can inform the digital documentation, historical reconstruction, spatial analysis, and remote access of other large-scale linear heritage systems, including railways, canals, and defensive networks.

From an application perspective, the integrated InfraHBIM/HBIM–GIS product supports heritage management and professional research, and it also contributes to the community governance and public education. For heritage owners and management authorities, the integrated database can support core tasks such as documentation, condition assessment, conservation planning, and long-term monitoring, thereby improving the continuity and precision of the heritage management. For engineers, architects, urban planners, and researchers, the proposed workflow is transparent, scalable, and reusable. It facilitates interdisciplinary collaboration and multi-source data sharing, and it provides methodological support for the digital reconstruction and analysis of comparable assets. For public and educational users, the WebGIS-based platform enables remote exploration and improves the access to the archival materials, supporting cultural dissemination, teaching, and public participation. Moreover, for heritage sites that already operate mature two-dimensional WebGIS access platforms, the technical pathway presented here offers a practical reference for moving from two-dimensional presentation and information query towards three-dimensional heritage management with diachronic representation.

Future work will extend the temporal sequence and documentation scope established in this study. First, additional InfraHBIM models will be developed to reconstruct the bridge construction period and to reveal key developments during design and building processes. Second, an InfraHBIM model representing the bridge condition surveyed in the summer of 2024 will be created to strengthen the contemporary record. These extensions will enhance the temporal continuity of the digital archive and provide more comprehensive data support for the sustainable management, long-term research, and public communication of this important infrastructure heritage.

Appendix A. Geometric accuracy assessment of HBIM models of the harbin-side blockhouses (WLMBHR0892BF and WLMBHR0892CF)

This appendix has reported the geometric accuracy assessment of HBIM models for the Harbin-side lockhouses (WLMBHR0892BF and WLMBHR0892CF), processed using the same workflow described for Harbin-side blockhouse (WLMBHR0892AF) in the main text. For consistency, all metrics follow the same definitions adopted in the Sect. "Geometric accuracy assessment of HBIM models".

Following the same evaluation procedure, the photogrammetric quality of the two blockhouses has been assessed in terms of bundle adjustment precision, camera self-calibration stability, and theoretical camera geolocation accuracy. For both buildings, a total of 17,115 tie points has been extracted, resulting in a bundle block adjustment (BBA) reprojection error of 0.29 pixels, which has indicated a higher level of internal consistency compared to WLMBHR0892AF. Considering a ground sampling distance (GSD) of 0.9 cm per pixel, this corresponds to an object-space precision of approximately 0.3 cm, indicating a high level of internal geometric consistency.

The estimation errors of the intrinsic camera parameters, including focal length and principal point, have ranged between 0.09 and 0.14 pixels, confirming stable self-calibration performance. The theoretical accuracy of camera absolute geolocation has shown larger variations, with average XY plane errors of 0.41 m and 0.36 m for WLMBHR0892BF and WLMBHR0892CF respectively, and vertical errors of approximately 0.88 m for both. These results have been consistent with the imaging conditions described for the Manzhouli-side blockhouse and have indicated that the photogrammetric point clouds of two blockhouses exhibit similar local variations in accuracy while maintaining adequate internal geometric stability.

After the coarse alignment, the 50% overlap region between the photogrammetric point clouds (PC1) and HBIM-derived point clouds (PC2) has been selected for fine registration. Iterative Closest Point (ICP) refinement within this area has yielded Root Mean Squared Error (RMSE) values of 0.07 m and 0.08 m. Based on the identification of the maximum thresholds (D_{max}) obtained from the bidirectional Cloud-to-Cloud Distance (C2C) analysis, occluded and poorly reconstructed regions have been removed to ensure that the comparison is restricted to reliable areas (Table 8 and Fig. 20).

A core point set of PC1 (PC1_Core) has been generated through spatial subsampling with a minimum spacing of 0.10 m to ensure a representative and noise-resistant distribution. Surface normals have been estimated using a multiscale neighbourhood with a normal scale of 0.20 m. The Multiscale Model to Model Cloud Comparison (M3C2) distances have then been computed within a search cylinder of 8 cm radius and 1.5 m maximum depth, while incorporating a registration error of 7 cm to account for alignment uncertainty.

Within the validated region, M3C2 metrics have indicated mean absolute deviations of 0.001 m and 0.002 m, standard deviations of 0.22 m and 0.16 m, and RMSE values of about 0.22 m for both datasets. Most distances have fallen within −0.45 to +0.45 m and −0.33 to +0.33 m, with the remaining outliers corresponding to residual data gaps or localized modelling inconsistencies. Compared with WLMBHR0892AF, these results demonstrate a similar level of geometric agreement between the HBIM models and the photogrammetric point clouds. Minor differences in the spread of the distance distributions mainly reflect variations in photogrammetric coverage and modelling complexity rather than systematic modelling errors. Overall, the outcomes for Harbin-side blockhouses confirm that the proposed workflow remains robust across different structures and yields consistent accuracy within reliably captured regions.

Table 8 Bidirectional cloud-to-cloud distance (C2C) metrics between the photogrammetric point clouds (PC1) and HBIM-derived point clouds (PC2) for Blockhouses WLMBHR0892BF and WLMBHR0892CF

Blockhouse's ID	PC1's scale (Points)	C2C direction	Mean (m)	Std. dev. (m)	Dmax (m)
WLMBHR0892BF	1,810,779	PC2 → PC1	0.36	0.32	0.80
		PC1 → PC2	0.10	0.08	0.25
WLMBHR0892CF	1,799,839	PC2 → PC1	0.39	0.37	0.75
		PC1 → PC2	0.09	0.08	0.16

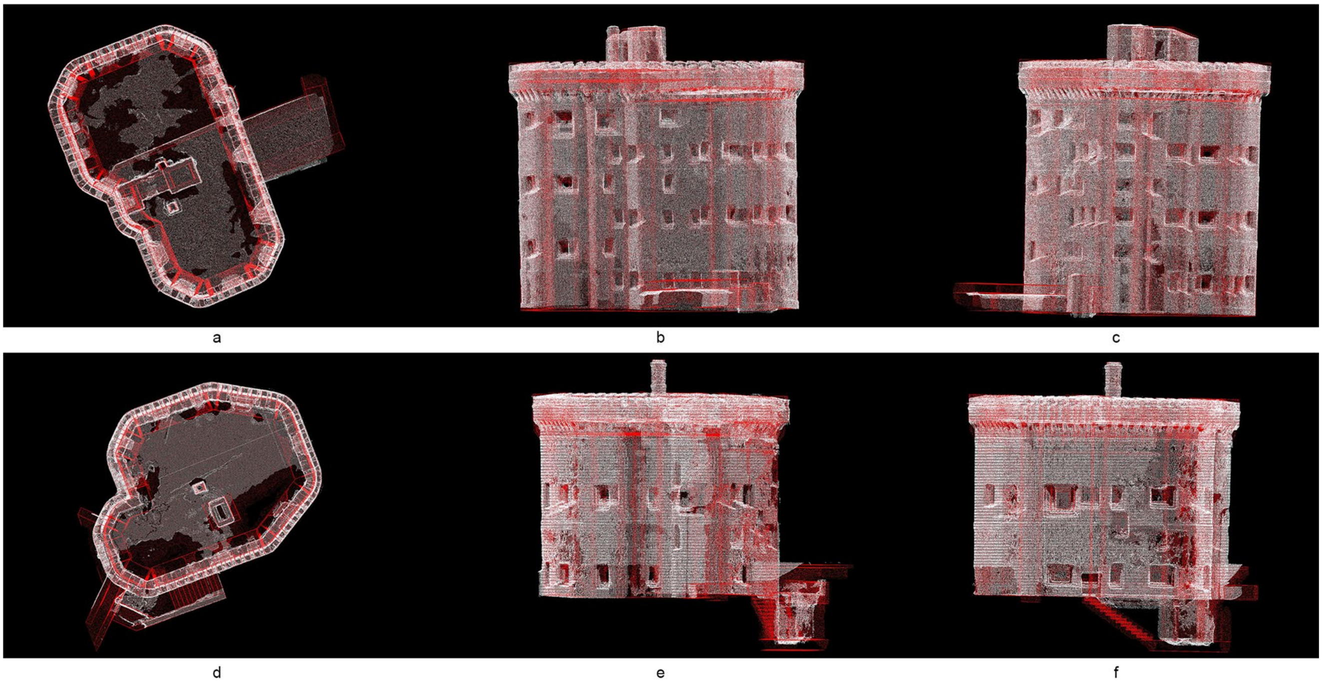

Fig. 20 Extraction of the reliable region for geometric comparison from the 50% valid overlap area between PC1 and PC2 of the blockhouses WLMBHR0892BF and WLMBHR0892CF: (**a**) and (**d**) Top view; (**b**) and (**f**) Bridge-facing façade; and (**c**) and (**e**) River-facing façade

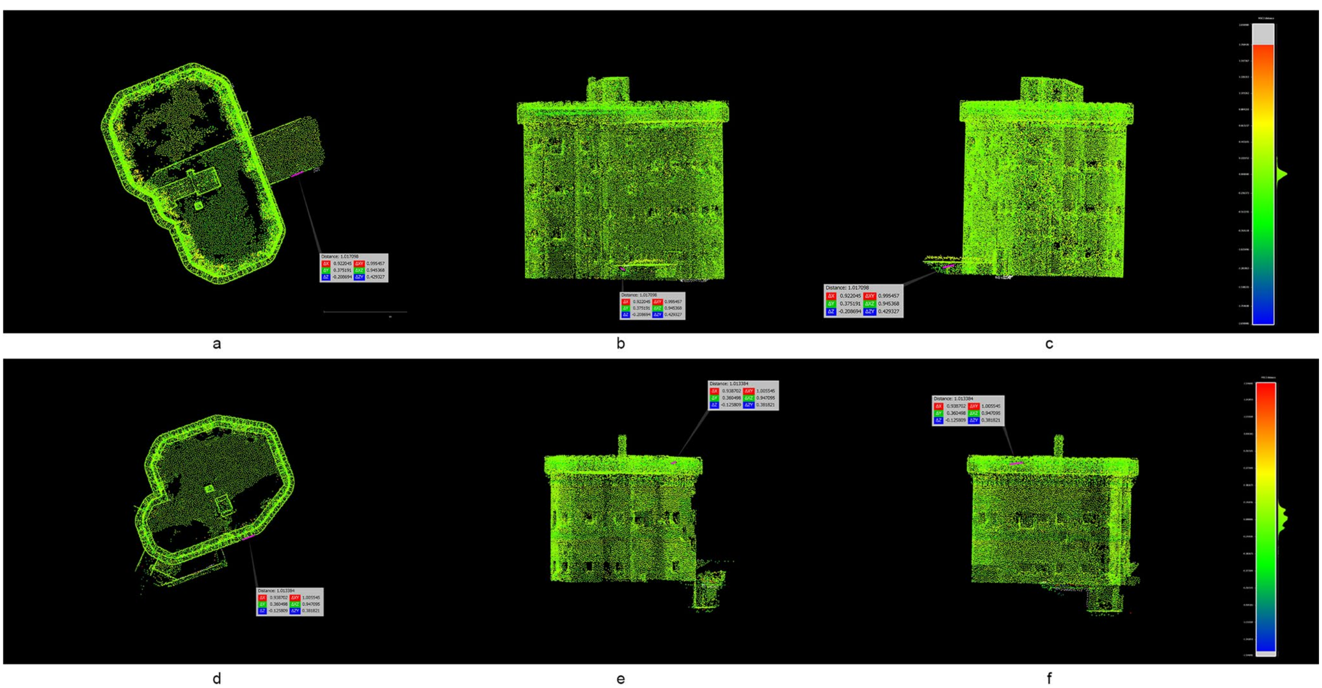

Fig. 21 M3C2-derived point-to-surface distances between PC1_Core and PC2: (**a**) and (**d**) Top-view, (**b**) and (**e**) Bridge-facing façade and (**c**) and (**f**) River-facing façade

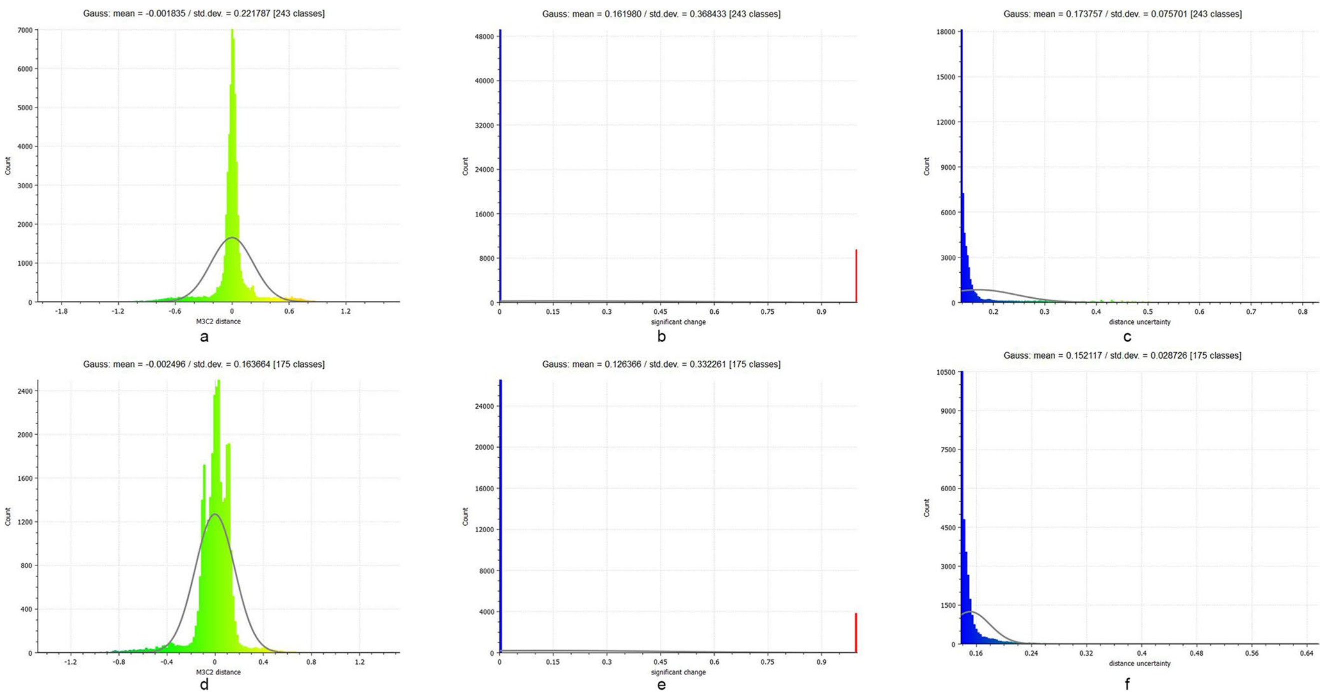

Fig. 22 M3C2-based geometric analysis results of the blockhouses WLMBHR0892BF and WLMBHR0892CF: (**a**) and (**d**) Distance histogram, (**b**) and (**e**) Significant change histogram, and (**c**) and (**f**) Distance uncertainty histogram

Acknowledgements The China Scholarship Council supported this work. The assistance provided by Prof. Yan Wang of the School of Architecture and Design, Harbin Institute of Technology.

Author contributions Xu participated in all stages of the study, prepared the figures, and wrote the main manuscript. Zhang assisted with the field surveying. Garramone supported the development of the HBIM model. Li contributed to the visualization of results through WebGIS publication. Scaioni provided key suggestions for assessing the geometric accuracy of the HBIM model, offered overall guidance, and reviewed the entire manuscript.

Funding Open access funding provided by Politecnico di Milano within the CRUI-CARE Agreement. This work was supported by the China Scholarship Council.

Data availability The Copernicus Global Digital Elevation Model (GLO-30) used in this study is publicly available from the European Space Agency at: https://doi.org/10.5270/ESA-c5d3d65. The p rovincial boundary data of China were obtained from the National Geomatics Center of China and can be accessed via the Tianditu platform (https://cloudcenter.tianditu.gov.cn/administrativeDivision). The point cloud and other datasets supporting the findings of this study were used under license for the current research and are therefore not publicly available. The integrated data results of this study can be remotely accessed via desktop at the following link: https://arcg.is/0aeLyK0.

Declarations

Competing interests The authors declare no competing interests.

Clinical trial number Not applicable.

References

Agisoft LLC (2024) Agisoft Metashape (Version 2.2.0)

American Institute of Architects (AIA) (2013) G202TM–2013. Project building information modeling protocol form. https://aia-acd.appcropolis.net/instructions_g202-2013/

Anon (1904) Album of structures of the Chinese Eastern Railway (Альбом сооружений Китайской Восточной железной дороги) (1897–1903). Fisher (Фишер), Moscow (Москва)
Anon (1919) Views of the Chinese Eastern Railway: General View of the Hingan Railway-Loop. DeGolyer Library, Southern Methodist University. Accessed 24 April 2024. https://digitalcollections.smu.edu/digital/collection/eaa/id/1550
Anon (1920) An Lien Bridge Near Harubin (哈爾賓松花江の大鉄橋).Main Library, Kyoto University. Accessed 05 March 2025. https://rmda.kulib.kyoto-u.ac.jp/en/item/rb00030914
Anon (1930) Harbin: Iron-bridge of R., Sungarri, Harbin. Manchukuo National Government Postcard (Taisho Photo Art Studio) (满洲国国政明信片 (大正写真工芸所)). Main Library, Kyoto University. Accessed 05 March 2025. https://rmda.kulib.kyoto-u.ac.jp/en/item/rb00030408
Anon (2019a) Bridge over the Sungari I (Мост через Су нгари I) (1920–1930). Retro View of Mankind's Habitat. Accessed 06 November 2024. https://pastvu.com/p/967756
Anon (2019b) Guard blockhouse of the Chinese Eastern Railway near the bridge over the Sungari River (Охранный блокгауз КВЖД у моста через р. Сунгари) (1918–1920). Retro View of Mankind's Habitat. Accessed 06 November 2024. https://pastvu.com/p/967499
Anon (2019c) Guard blockhouse of the Chinese Eastern Railway near the Sungari I Bridge (Охранный блокгауз КВЖД у моста Сунгари I) (1918–1922). Retro View of Mankind's Habitat. Accessed 6 Nov 2024. https://pastvu.com/p/967757
Antonopoulou S, Bryan P (2017) BIM for heritage: developing a historic building information model. Historic England, London
Arayici Y, Counsell J, Mahdjoubi L et al (2017) Heritage building information modelling. Routledge, London
Autodesk Inc. (2024) Autodesk ReCap (Version 25.1.0.307)
Autodesk Inc. (2025a) Levels of Development in BIM. Accessed 05 March 2025. https://www.autodesk.com/solutions/bim-levels-of-development?msockid=19dc33acd37866b123852490d2a5674a
Autodesk Inc. (2025b) Autodesk Revit (Version 2025)
Autodesk Inc. (2025c) Autodesk Viewer. Accessed 07 March 2025. https://viewer.autodesk.com/
Avilov R S (2024) Defensive construction on the Chinese Eastern Railway on the eve of and during the first world war: issues of financing (Оборонительное строительство на КВЖД накануне и во время Первой мировой войны: проблемы финансирования). New Historical Bulletin (Новый исторический вестникProcess), 2(80): 6–27. https://doi.org/10.54770/20729286_2024_2_6
Barazzetti L (2021) Integration between building information modeling and geographic information system for historic buildings and sites: Historic-BIM-GIS. ISPRS Ann Photogramm Remote Sens Spatial Inf Sci. https://doi.org/10.5194/isprs-annals-VIII-M-1-2021-41-2021
Barrile V, Bernardo E, Candela G et al (2020) Road infrastructure heritage: from scan to InfraBIM. WSEAS Transactions on Environment and Development 16:633–642. https://doi.org/10.37394/232015.2020.16.65
Bouzas Ó, Cabaleiro M, Conde B et al (2022) Structural health control of historical steel structures using HBIM. Autom Constr 140:104308. https://doi.org/10.1016/j.autcon.2022.104308
Brumana R, Della Torre S, Previtali M et al (2018) Generative HBIM modelling to embody complexity (LOD, LOG, LOA, LOI): surveying, preservation, site intervention—the basilica di Collemaggio (L'Aquila). Appl Geomat 10:545–567. https://doi.org/10.1007/s12518-018-0233-3
Bruno N, Rechichi F, Achille C et al (2020) Integration of historical GIS data in a HBIM system. Int Arch Photogramm Remote Sens Spatial Inf Sci. https://doi.org/10.5194/isprs-archives-XLIII-B4-2020-427-2020
buildingSMART International (2013) IFC 4. Accessed 14 June 2025. https://standards.buildingsmart.org/IFC/RELEASE/IFC4/FINAL/HTML/
Carrasco CA, Lombillo I, Sánchez-Espeso J (2022) Methodology for the generation of 3D city models and integration of HBIM models in GIS: case studies. VITRUVIO - Int J Architectural Technol Sustain 7:74–87. https://doi.org/10.4995/vitruvio-ijats.2022.18808
Chinese Eastern Railway (190?) Album of structures and standard drawings of the Chinese Eastern Railway (Альбом сооружений и типовых чертежей Китайской Восточной железной дороги) (1897–1903). Moscow (Москва)
CloudCompare Development Team (2025) CloudCompare (Version 2.14.alapha)
Colucci E, De Ruvo V, Lingua A et al (2020) HBIM-GIS integration: from IFC to CityGML standard for damaged cultural heritage in a multiscale 3D GIS. Appl Sci-Basel 10:1356. https://doi.org/10.3390/app10041356
Conti A, Fiorini L, Massaro R et al (2022) HBIM for the preservation of a historic infrastructure: the Carlo III bridge of the Carolino Aqueduct. Appl Geomat 14:41–51. https://doi.org/10.1007/s12518-020-00335-2
Cursi S, Martinelli L, Paraciani N et al (2022) Linking external knowledge to heritage BIM. Autom Constr 141:104444. https://doi.org/10.1016/j.autcon.2022.104444
Di Donato D, Morganti R, Tosone A, Abita M (2022) Procedural modelling for HBIM of Italian railways iron bridges. Int Arch Photogramm Remote Sens Spatial Inf Sci. https://doi.org/10.5194/isprs-archives-XLVI-2-W1-2022-207-2022
Donato V, Biagini C, Bertini G, Marsugli F (2017) Challenges and opportunities for the implementation of H-BIM with regards to historical infrastructures: a case study of the Pponte Ggiorgini in Ccastiglione Ddella Ppescaia (Grosseto – Italy). Int Arch Photogramm Remote Sens Spatial Inf Sci. https://doi.org/10.5194/isprs-archives-XLII-5-W1-253-2017
Esri (2024a) ArcGIS Pro (Version 3.4)
Esri (2024b) ArcGIS Online
European Space Agency (2024) Copernicus global digital elevation model (GLO-30). https://doi.org/10.5270/ESA-c5d3d65
Garozzo R, Santagati C (2021) Digital survey AI and semantics for railway masonry bridges health assessment. Int Arch Photogramm Remote Sens Spatial Inf Sci. https://doi.org/10.5194/isprs-archives-XLVI-M-1-2021-249-2021
Garramone M, Jovanovic D, Oreni D et al (2023) Basilica di san giacomo in como (Italy): drawings and HBIM to manage archeological, conservative and structural activities. Int Arch Photogramm Remote Sens Spatial Inf Sci. https://doi.org/10.5194/isprs-archives-XLVIII-M-2-2023-653-2023
Garramone M, Moretti N, Scaioni M et al (2020) BIM and GIS integration for infrastructure asset management: a bibliometric analysis. ISPRS Ann Photogramm Remote Sens Spatial Inf Sci. https://doi.org/10.5194/isprs-annals-VI-4-W1-2020-77-2020
Garramone M, Scaioni M (2023) A BIM/GIS digitalization process to explore the potential of disused railways in Italy. Int Arch photogramm remote Sens Spatial Inf Sci. https://doi.org/10.5194/isprs-archives-XLVIII-5-W2-2023-37-2023
Gómez A, Adineh A, Rahrig M, Lerma JL (2024) Narrating Serranos bridge evolution in Valencia (1500–2022) using historic building information modelling and historical data. Remote Sens 16:310. https://doi.org/10.3390/rs16020310
Google (2025) Google Earth Pro (Version 7.3.6.10201)
Granshaw SI (2018a) RPV, UAV, UAS, RPAS … or just drone? Photogramm Rec 33:160–170. https://doi.org/10.1111/phor.12244
Granshaw SI (2018b) Structure from motion: origins and originality. Photogramm Rec 33:6–10. https://doi.org/10.1111/phor.12237

Lague D, Brodu N, Leroux J (2013) Accurate 3D comparison of complex topography with terrestrial laser scanner: application to the Rangitikei canyon (N-Z). ISPRS J Photogramm Remote Sens 82:10–26. https://doi.org/10.1016/j.isprsjprs.2013.04.009

León-Robles CA, Reinoso-Gordo JF, González-Quiñones JJ (2019) Heritage building information modeling (H-BIM) applied to a stone bridge. ISPRS Int J Geo-Inf 8:121. https://doi.org/10.3390/ijgi8030121

Luhmann T, Robson S, Kyle S, Boehm J (2020) Close-range photogrammetry and 3D Imaging. De Gruyter, Berlin, Boston. https://doi.org/10.1515/9783110607253

Maset E, Matellon A, Gubiani S, Visintini D, Beinat A (2025) Introducing SLAM-based portable laser scanning for the metric testing of topographic databases. Remote Sens 17:3316. https://doi.org/10.3390/RS17193316

Matrone F, Colucci E, Iacono E, Ventura GM (2023a) The HBIM-GIS main10ance platform to enhance the maintenance and conservation of historical built heritage. Sensors 23:8112. https://doi.org/10.3390/s23198112

Matrone F, Felicetti A, Paolanti M, Pierdicca R (2023b) Explaining AI: understanding deep learning models for heritage point clouds. ISPRS Ann Photogramm Remote Sens Spatial Inf Sci. https://doi.org/10.5194/isprs-annals-X-M-1-2023-207-2023

Murphy M, McGovern E, Pavia S (2009) Historic building information modelling (HBIM). Struct Surv 27:311–327. https://doi.org/10.1108/02630800910985108

National Geomatics Center of China (2025) Administrative boundary visualization. Accessed 10 November 2025. https://cloudcenter.tianditu.gov.cn/administrativeDivision

Nilus EX (1923) Historical overview of China Eastern Railway (1896–1923). Printing Houses of the Chinese Eastern Railway and the Ozo Partnership (Типографии Кит. Вост. жел. дор. и Т-ва Озо)

Pepe M, Costantino D, Alfio VS et al (2021) Scan to BIM for the digital management and representation in 3D GIS environment of cultural heritage site. J Cult Herit 50:115–125. https://doi.org/10.1016/j.culher.2021.05.006

Phot Khosita (1901) Album of Views of the Chinese Eastern Railway (Альбом видов Китайской восточной железной дороги). Place of publication not identified (Б.м.)

Podolsky BM (1910) Chinese eastern railway (Китайская Восточная железная дорога). Harbin (Харбин)

Pomerleau F, Colas F, Siegwart R, Magnenat S (2013) Comparing ICP variants on realworld data sets. Auton Robot 34:133–148. https://doi.org/10.1007/s10514-013-9327-2

Pozzoni L, Barazzetti L, Cuca B, Oteri AM (2024) An Integrated HBIM-GIS digital environment for heritage preservation and enhancement in the inner Italian territory. Int Arch Photogramm Remote Sens Spatial Inf Sci. https://doi.org/10.5194/isprs-archives-XLVIII-2-W4-2024-357-2024

Previtali M, Barazzetti L, Banfi F, Roncoroni F (2019) Informative content models for infrastructure load testing management: the Azzone Visconti bridge in Lecco. Int Arch Photogramm Remote Sens Spatial Inf Sci. https://doi.org/10.5194/isprs-archives-XLII-2-W11-995-2019

QGIS Association (2023) QGIS (Version 3.30.2)

Rio ID, Cabaleiro M, Conde B et al (2020) HBIM application to historical steel structures. the case study of Llapela Bridge. Proceedings of the 5th World Congress on Civil Structural, and Environmental Engineering (CSEE'20), Virtual Conference, October 2020, Paper No. ICSECT 160 https://doi.org/10.11159/icsect20.160

Schmidt F (2019) GEOSETTER (Version 3.5.3)

The Compilation Committee of the Harbin Railway Admission (1999) Historical records of the Harbin Railway Admission (哈尔滨铁路分局志) (1896–1995). China Railway Publishing House, Beijing (中国铁道出版社，北京)

The State Council of the People's Republic of China (2013) The seventh batch of national key cultural heritage protection units (第七批全国重点文物保护单位名单). Accessed 14 March 2025. http://www.ncha.gov.cn/art/2013/5/3/art_722_107827.html

United Nations (2015) Sustainable Development Goals. Accessed 07 March 2025. https://sdgs.un.org/goals

Wang H, Pan Y, Luo X (2019) Integration of BIM and GIS in sustainable built environment: a review and bibliometric analysis. Autom Constr 103:41–52. https://doi.org/10.1016/j.autcon.2019.03.005

Winiwarter K, Anders B, Höfle B, (2021) M3C2-EP: Pushing the limits of 3D topographic point cloud change detection by error propagation. ISPRS J Photogrammetry Remote Sens 178:240–258. https://doi.org/10.1016/j.isprsjprs.2021.06.011

Xu J, Garramone M, Scaioni M (2024) Integration of HGIS/HBIM to reveal and reconstruct the vanished metal bridge heritage of the Chinese Eastern Railway Main Line. Int Arch Photogramm Remote Sens Spatial Inf Sci. https://doi.org/10.5194/isprs-archives-XLVIII-4-W11-2024-161-2024

Xu J, Garramone M, Scaioni M (2025a) Application and comparison of different HBIM/GIS integration methods in railway infrastructure heritage: a case study of the Muling River Bridge along the Chinese Eastern Railway Main Line. Int Arch Photogramm Remote Sens Spatial Inf Sci. https://doi.org/10.5194/isprs-archives-XLVIII-M-9-2025-1631-2025

Xu J, Garramone M, Scaioni M (2025b) HBIM-GIS integration of infrastructure heritage with complex documentation and conservation states: methodology and application to the historic bridges along Chinese Eastern Railway Main Line. ISPRS Ann Photogramm Remote Sens Spatial Inf Sci. https://doi.org/10.5194/isprs-annals-X-5-W3-2025-49-2025

Xu J, Garramone M, Wang Y, Scaioni M (2023a) Integration of HBIM/GIS to preserve infrastructure heritage along the Chinese Eastern Railway. Int Arch Photogramm Remote Sens Spatial Inf Sci. https://doi.org/10.5194/isprs-archives-XLVIII-M-2-2023-1645-2023

Xu J, Scaioni M (2023b) A brief feasibility analysis of HBIM/GIS integration in the infrastructure heritage conservation: the case of the Chinese Eastern Railway (CER) main line. Int Arch Photogramm Remote Sens Spatial Inf Sci. https://doi.org/10.5194/isprs-archives-XLVIII-5-W2-2023-117-2023

Yang X, Grussenmeyer P, Koehl M et al (2020) Review of built heritage modelling: integration of HBIM and other information techniques. J Cult Heri 46:350–360. https://doi.org/10.1016/j.culher.2020.05.008

Zhu J, Wu P (2022) BIM/GIS data integration from the perspective of information flow. Autom Constr 136:104166. https://doi.org/10.1016/j.autcon.2022.104166